Topography of corticopontine projections is controlled by postmitotic expression of the area-mapping gene Nr2f1

Chiara Tocco[1]*, Martin Øvsthus[2]*, Jan G. Bjaalie[2], Trygve B. Leergaard[2#], Michèle Studer[1#]

[1]*Université Côte d'Azur, CNRS, Inserm, iBV, France*

[2]*Institute of Basic Medical Sciences, University of Oslo, Oslo, Norway*

*These authors have contributed equally to the study.

#Co-last authors.

[@]Corresponding author:

Michèle Studer
iBV - Institut de Biologie Valrose
Univ. Côte d'Azur
Centre de Biochimie ; UFR Sciences
Parc Valrose, 28 avenue Valrose
06108 Nice Cedex 2
France
Tel.: +33 489150720
e-mail: Michele.studer@unice.fr

SUMMARY

Axonal projections from layer V neurons of distinct neocortical areas are topographically organized into discrete clusters within the pontine nuclei during the establishment of voluntary movements. However, the molecular determinants controlling corticopontine connectivity are insufficiently understood. Here, we show that an intrinsic cortical genetic program driven by Nr2f1 graded expression is directly implicated in the organization of corticopontine topographic mapping. Transgenic mice lacking cortical expression of *Nr2f1* and exhibiting areal organization defects were used as model systems to investigate the arrangement of corticopontine projections. Combining three-dimensional digital brain atlas tools, *Cre*-dependent mouse lines, and axonal tracing, we show that *Nr2f1* expression in postmitotic neurons spatially and temporally controls somatosensory topographic projections, whereas expression in progenitor cells influences the ratio between corticopontine and corticospinal fibers passing the pontine nuclei. We conclude that cortical gradients of area patterning genes are directly implicated in the establishment of a topographic somatotopic mapping from the cortex onto pontine nuclei.

Keywords: corticopontine topography, layer V neurons, area mapping genes, Nr2f1, mouse models, *Thy1*-e*YFP-H* reporter line, pontine nuclei, 3D data points, interactive 3D viewer tools, anterograde fluorescent tracing

INTRODUCTION

Neuronal populations responsible for fine motor coordination are arranged in topographically organized maps in the neocortex and cerebellum exemplified by different body parts being represented in largely continuous maps in the somatosensory cortex (Chapin and Lin, 1984; Fabri and Burton, 1991; Welker, 1971; Woolsey and Van der Loos, 1970), and discontinuous, fractured maps in the cerebellum (Bower, 2011; Bower et al., 1981; Bower and Kassel, 1990; Leergaard et al., 2006; Nitschke et al., 1996; Shambes et al., 1978). The intercalated regions of this network, including the pontine nuclei, deep cerebellar nuclei, and the thalamus, receive and integrate signals ultimately resulting in coordinated and seamlessly executed behaviors (Buckner, 2013; Peterburs and Desmond, 2016; Stoodley and Schmahmann, 2010), including fine voluntary movements (Badura et al., 2013; Mottolese et al., 2013).

The pontine nuclei constitute the major synaptic relay for cerebro-cerebellar signals (Brodal and Bjaalie, 1992; Lemon, 2008; Mihailoff et al., 1985). Axonal projections originating from layer V pyramidal neurons across the neocortex are distributed in topographically organized clusters within the pontine nuclei, as shown in monkey (Brodal, 1978; Schmahmann and Pandya, 1997), cat (Bjaalie and Brodal, 1997), rat (Leergaard et al., 2000a; Leergaard et al., 2000b), and to some extent also in mice (Henschke and Pakan, 2020; Inoue et al., 1991; Proville et al., 2014). Within the pontine nuclei, the three-dimensional (3D) arrangement of clustered terminal fields, well described in rats, both preserves the overall topographical relationships of the cortical maps, but also partially overlap and introduce new spatial proximities among projections from different cortical areas (Bjaalie and Brodal, 1989; Leergaard, 2003; Leergaard and Bjaalie, 2007). The somatosensory system constitutes the largest proportion of the cerebro-cerebellar system, with highly organized projections from the primary somatosensory cortex to central parts of the pontine nuclei (Leergaard et al., 2000a; Leergaard et al., 2000b; Leergaard et al., 2004).

To date, the mechanisms responsible for establishing the topographic map between the neocortex and pontine nuclei are poorly understood. The leading proposition, referred to as chrono-architectonic hypothesis, postulates that the complex 3D topography is a product of straightforward spatio-temporal gradients, possibly combined with non-specific chemo-attractive mechanisms (Leergaard, 2003; Leergaard and Bjaalie, 2007; Leergaard et al., 1995).

Recent new discoveries open the possibility that other mechanisms are also in action during the establishment of the corticopontine maps. Several lines of evidence point to a functional role of gradients in gene expression during topography of sensory maps in several systems (D'Elia and Dasen, 2018; Erzurumlu et al., 2010; Fritzsch et al., 2019; McLaughlin and O'Leary, 2005), but whether this process is also operative during establishment of corticopontine topography is not completely understood. A recent study has shown that postmitotic graded expression of the HOX gene *Hoxa5* is directly involved in imparting an anterior to posterior identity to pontine neurons and attract corticopontine axons (Maheshwari et al., 2020), suggesting that pontine nuclei could play an instructive role in establishing topographical organization. Whether expression in gradients of molecular factors along the antero-posterior or medio-lateral axes of the cerebral cortex also intrinsically determine the topography of corticopontine projections is still not known. Layer V neurons from the anterolateral cerebral cortex project to the central regions of the pontine nuclei, while more medially located cortical regions project to more external parts; projections from motor areas are distributed more medially and rostrally, with projections from somatosensory areas reaching the middle and caudal parts of the pontine nuclei. Finally, auditory and visual cortical projections innervate the dorsolateral regions of the pontine nuclei (Leergaard et al., 2004; Leergaard and Bjaalie, 2007). The fine-tuned and precise topography between the cortex and pontine nuclei leaves open the possibility for cortical neurons being intrinsically programmed to target specific groups of pontine neurons, possibly coupling both intrinsic and extrinsic mechanisms in directing proper topographical innervation to the pontine nuclei.

A new theme of cortical patterning emerges, in which genetic factors direct the spatial and temporal establishment of topographically organized axonal connections between the cortex and subcortical brain regions (Cadwell et al., 2019). Area mapping genes are expressed in gradients along the different axes of the cortical primordium, are known to modulate the size and position of future cortical areas (Alfano and Studer, 2012; Cadwell et al., 2019; O'Leary and Sahara, 2008), and to determine areal fate and regulate expression of downstream molecules that in turn control the topographic organization of synaptic inputs and outputs of related structures (Assimacopoulos et al., 2012; Greig et al., 2013). These genes represent therefore good candidates for modulating topographic mapping. In mice, the Nr2f1 gradient expression appears to be a particularly strong candidate for having a formative role during

103 the establishment of topographic maps (Armentano et al., 2007b; Liu et al., 2000; Zhou et al.,
104 2001). For instance, Nr2f1 (also known as COUP-TFI) is expressed in cortical progenitor cells
105 from embryonic day E9.0 in a high caudo-lateral (future sensory) to low rostro-medial (future
106 motor) gradient fashion, and the gradient expression is maintained in postmitotic
107 descendants as well as postnatally when the cortical area map is completed (Bertacchi et al.,
108 2019; Flore et al., 2017; Tomassy et al., 2010). Previous studies show that Nr2f1 promotes
109 somatosensory (S1) by repressing motor identity in postmitotic neurons and in its absence
110 area size and thalamocortical topography are both shifted (Alfano et al., 2014a; Armentano
111 et al., 2007b; Bertacchi et al., 2019). We thus hypothesized that Nr2f1 could represent one of
112 these factors able to control topographic corticopontine mapping during corticogenesis.
113
114 To this purpose, we made use of cortico-specific *Nr2f1* conditional knockout mice as an i*n vivo*
115 model system and a paradigm to investigate the contribution of cortical genetic programs in
116 the establishment of topographic corticopontine projections. Two distinct conditional mouse
117 lines, in which *Nr2f1* is knocked out in either cortical progenitor cells or postmitotic cortical
118 neurons (Alfano et al., 2014b; Armentano et al., 2007b) were crossed to the *Thy1*-e*YFP-H*
119 reporter line (Feng et al., 2000), in which YFP is highly expressed in cortical layer V pyramidal
120 neurons and their axonal projections (Porrero et al., 2010). The distribution of fluorescent YFP
121 signals as well as anterogradely labelled corticopontine projections were evaluated by side-
122 by-side comparison of spatially corresponding microscopic images of conditional knock-out
123 and control littermate animals, and by 3D visualization of extracted point-coordinated data
124 representing labelling (see flowchart in **Figure 1**). Our data indicate that cortical Nr2f1
125 expression plays a dual role in controlling the spatio-temporal development of corticopontine
126 projections. While early expression in progenitor cells influences the ratio between
127 corticofugal fibers passing the pontine nuclei, loss of solely postmitotic late expression
128 specifically affects topographic pontine mapping. Overall, our results demonstrate that
129 intrinsic genetic programs and postmitotic graded expression of cortical area mapping genes
130 are implicated in the spatio-temporal establishment of area-specific targeting of
131 corticopontine neurons.

RESULTS

Benchmark 3D topographic organization of corticopontine projections in wild-type mice

To first establish a 3D reference of the topographical organization of corticopontine projections in normal adult (wild-type) mice, we used tract tracing data from the *Allen Institute Mouse Brain Connectivity Atlas* (Wang et al., 2020), see flowchart in **Figure 1A**. These data allowed us to visualize the spatial distribution of the pontine projections of motor and somatosensory neocortical areas. Corticopontine projections digitized from sagitally-oriented microscopic images (matching the orientation used for our experimental data, see below) were co-visualized as 3D data points in a 3D viewer tool (see examples shown in **Figure 2A-D**). Experimental data were selected and colored according to tracer injection localizations in the cerebral cortex, to first visualize and compare the pontine distribution of corticopontine projections from motor and somatosensory areas, and secondly to determine the organization of projections arising from progressively more medial and caudal locations in the cerebral cortex, following the cortical neurogenetic gradient that ripples out from the anterolateral cortex (Leergaard and Bjaalie, 2007; Smart, 1984). Our findings confirm that the somatosensory and motor neurons of the mouse cortex project to largely separate parts of the pontine nuclei (Henschke and Pakan, 2020; Inoue et al., 1991; Proville et al., 2014), with clustered terminal fields that are topographically distributed in the same concentric fashion (**Figure 2L-P**), as previously reported in rats (Leergaard et al., 2000a; Leergaard and Bjaalie, 2007). The 3D point data presented here are also used below as supplementary control data, and as benchmarks for interpreting YFP expression and tract-tracing results in *Nr2f1* mutant mice.

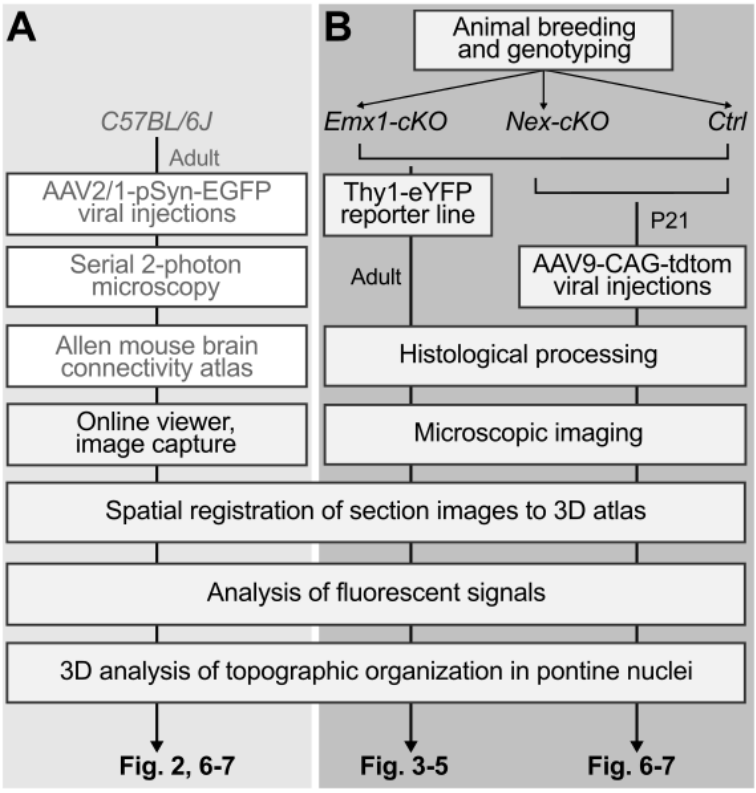

Figure 1. Experimental and analytic workflow. *(**A**) Workflow for generating a 3D control topographic map of corticopontine projections using public tract tracing data (https://connectivity.brain-map.org/), mapped and compared in a 3D reference atlas space. In light gray text and white boxes, the steps performed by the Allen institute (**B**) The middle and right column represent the two paradigms investigated in conditional mouse models, with the analytic steps performed in adult control, Emx1-cKO and Nex-cKO mutant animals (middle column), and the tract tracing study of the 3D topography of motor and somatosensory corticopontine projections in young control and Nex-cKO mutant animals (right column). All images were spatially registered to the Allen mouse brain atlas (CCFv3; Wang et al., 2020) prior to analyses, to facilitate comparison of images and spatial distribution patterns. Results are shown in Figures 2-7.*

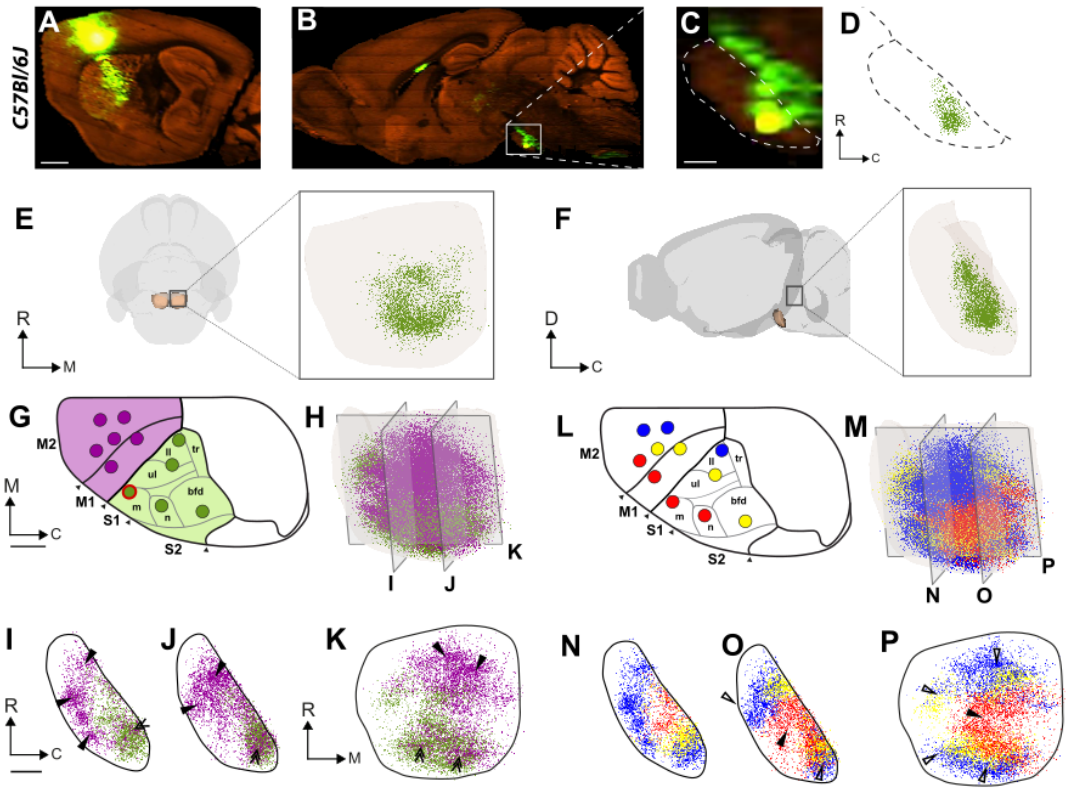

Figure 2. Topographical organization of corticopontine projections in wild-type mice. *(**A-D**) Representative example illustrating the data acquisition of corticopontine projections labelled by viral tracer injection in the S1 face representation in C57BL/6J mice from the Allen Mouse Brain Connectivity Atlas. **A** shows the localization of the injection site relative to the experiment indicated in red in panel **G**. **B** shows anterogradely labelled axons in the pontine nuclei (enlarged in **C**). **D** indicates semi-quantitatively recorded points corresponding to the density of labelling observed in **C**. Panels **E,F** show the 3D point populations recorded together with a transparent surface rendering of the right pontine nuclei, seen in view from ventral (**E**) and medial (**F**). The S1 corticopontine projections are distributed in dense clusters located centrally in the pontine nuclei. (**G-K** and **L-P**) 3D visualizations of point clouds representing spatial distribution of anterogradely labeled corticopontine axons derived from 11 experiments available in the Allen Mouse Brain Connectivity Atlas, injected with the anterograde tracer EGFP in the primary (M1)/secondary (M2) motor cortex (purple dots) or primary somatosensory (S1) cortex (green dots), at locations indicated with color coded circles in **G** and **L**. (**H, M**) 3D visualizations of all points in the right pontine nuclei, color coded as indicated in **G** and **L**. A grid of transparent grey planes indicate the position and orientation of ~100 µm thick digital slices cut with sagittal and frontal orientations through the point clouds, shown in **I-K**, and **N-P**. (**G-K**) Point clouds showing that motor and somatosensory areas largely target different parts of the pontine nuclei, with projections from M1 and M2 (purple dots) located more peripherally towards rostral, ventral, and medial than projections from S1 (green dots) as indicated by arrowheads in **I-K**, but also that motor and sensory projections overlap caudally in the pontine nuclei (double arrowheads in **I-K**). (**L-P**) 3D co-visualization of all data points color coded in red, yellow or blue according to the location of the cortical injection sites from anterolateral (red) progressively towards medial or posterior (yellow, blue). The slices through the point clouds reveal a concentric arrangement in the pontine nuclei, with projections from the anterolateral parts of the M1/M2 and S1 located centrally and medially (arrowheads in **O-P**), and projections from more medial and posterior cortical locations progressively shifted towards rostral, caudal, and lateral (unfilled arrowheads in (**O-P**). Abbreviations: bfd, barrel field; C, caudal; D, dorsal; ll, lower limb; m, mouth; M1, primary motor cortex; M2, secondary motor cortex; n, nose; R, rostral; S1, primary somatosensory cortex; S2, secondary somatosensory cortex, tr, trunk; ul, upper limb; V, ventral. Scale bars, 1 mm (**A, B**), 200 µm (**C,I**).*

193 **Area-specific layer V neuron distribution in cortices lacking Nr2f1**

194 To assess the influence of cortical area mapping on the establishment of topographical
195 organization in mouse corticopontine projections, we used *Nr2f1* deficient mice as
196 experimental model system and littermate controls (Alfano et al., 2014b; Armentano et al.,
197 2007b). To this purpose, we used two well-established conditional *Nr2f1* mouse mutants: the
198 *Nr2f1*$^{fl/fl}$*::Emx1-Cre* mouse, in which *Nr2f1* expression is abolished from early cortical
199 progenitor cells at mouse embryonic (E) age 9.5 (Armentano et al., 2007b), and the
200 *Nr2f1*$^{fl/fl}$*::Nex-Cre* mouse in which *Nr2f1* expression is inactivated at later stages (E11.5-E12),
201 solely in cortical postmitotic neurons (Alfano et al., 2014b; Goebbels et al., 2006). Both mouse
202 lines were crossed to the *Thy1-eYFP-H* reporter line to specifically restrict signal expression to
203 layer V pyramidal neurons, allowing labelling of subcortical projection neurons, including
204 corticospinal and corticopontine fibers (Harb et al., 2016; Porrero et al., 2010). For simplicity,
205 both lines will be named from here on *Emx1-cKO* and *Nex-cKO*, respectively (see workflow in
206 **Figure 1B**).

207 In agreement with the earlier detailed report by Porrero et al. (Porrero et al., 2010), we
208 observed substantial YFP signal expression in the hippocampus, tectum, and pontine nuclei,
209 as well as in the globus pallidus, claustrum, endopiriform nucleus, nucleus of the lateral
210 olfactory tract, mammillary nuclei, piriform area, and the substantia innominata in adult mice
211 (**Figure 3A**). Signal expression was also seen in the vestibular nuclei, deep cerebellar nuclei,
212 and cerebellum. Although signal expression was present in almost the same regions in 2-
213 months-old mutant mice as in controls, more detailed analysis of layer V expression in
214 neocortical areas revealed some distinct differences in the spatial distribution of *Emx1-cKO*
215 and *Nex-cKO* brains relative to their respective controls, and between the two conditional
216 lines. We used an ImageJ macro allowing automatic counting of spots by area of interest in
217 the brain. The spots, representing specific nuclei staining, were obtained by using a threshold
218 based on intensity and shape of the elements. The composite segmentation atlas was used to
219 create masks for the regions of interest (THIS ANALYSIS IS NOT YET IMPLEMENTED AND WILL
220 BE FINALIZED IN A NEW REVISED VERSION). This allowed to estimate the amount of signal
221 expression across the cerebral cortex, in areas defined by delineations derived from spatially
222 registered overlay images from the *Allen Mouse Brain Atlas* ((Wang et al., 2020); **Figure 1;**

223 **Figure 3B-D'**). In control animals, the distribution of YFP-expressing neurons followed a
224 rostrally high to caudally low gradient (**Figure 3A, B, B'**), in line with the physiological layer V
225 neuron distribution to contain representations of the trunk and limbs and to the earlier
226 documented high numbers of layer V neurons in the rostrally located motor areas (Polleux et
227 al., 1997; Porrero et al., 2010; Shepherd, 2009). Strong staining in these areas resulted in
228 bright signal expression in the cerebral peduncle and CST (**Figure 3A).** We first assessed the
229 spatial organization of YFP-expressing layer V cortical distribution in mutant adults compared
230 to control animals. The layer V gradient was disrupted in mutant animals and the YFP signal
231 more homogenously distributed along the anteroposterior axis and at both lateral and medial
232 levels (**Figures 3C, C' and D, D'**). Increased YFP expression was observed caudally in the
233 occipital and retrosplenial cortex in both groups of mutant mice, in conjunction with
234 decreased YFP signal in frontal areas, which was particularly more pronounced in *Nex-cKO*
235 than *Emx1-cKO* mice (**Figures 3B-F**). In line with previous studies (Alfano et al., 2014b;
236 Armentano et al., 2007a; Tomassy et al., 2010), the YFP signal in layer V was radially increased
237 in S1 of the *Emx1-cKO* cortex (**Figure 3B, C, F**), but no statistical difference compared to
238 controls was detected in S1 of *Nex-cKO* brains (**Figure 3B, D, F**). (THIS PARAGRAPH WILL BE
239 UPDATED IN ACCORDANCE WITH THE NEW ANALYSIS).

240 Together, these data suggest a different role for Nr2f1 in early progenitor cells (*Emx1-cKO*)
241 and late postmitotic neurons (*Nex-cKO*) in layer V areal distribution, particularly in M1 and S1
242 (**Figure 3F).** We next asked whether and how alterations in layer V organization observed in
243 the two mutant lines would be translated into layer V corticospinal projections and/or
244 corticopontine topographic mapping.

245
246 ***(A NEW FIGURE WILL BE PRESENTED IN THE REVISED VERSION) Figure 3 – Cortical distribution of YFP-***
247 ***positive layer V pyramidal neurons in control, Emx1-cKO and Nex-cKO adult brains.*** *(**A**) Fluorescence*
248 *microscopy image of a representative sagittal section from a Thy1-YFP-H mouse brain, showing widespread*
249 *YFP expression. (**B-D/B'-D'**) Fluorescence microscopy images from sagittal sections located laterally (**B-D**)*
250 *and more medially (**B'-D'**) in Ctrl, Emx1-cKO, and Nex-cKO brains, with custom made, spatially*
251 *corresponding CCFv3 atlas diagrams superimposed on the microscopic images to define the location of*
252 *different cortical areas. (**E**) Semi-quantitative scale used to score the amount of signal expression: 0,*
253 *attributed to absence of positive cells (not shown); 1, very few and sparse cells with low to medium signal*
254 *intensity; 2, moderate number of sparse cells with moderate to high signal intensity; 3, high number of*
255 *partially overlapping cells with high signal intensity; 4, very high number of extensively overlapping cells*
256 *with high to very high signal intensity. (**F**) Column graphs showing the scoring of YFP-H signal expression*
257 *across cortical areas in adult Ctrl (grey), Emx1-cKO (light blue) and Nex-cKO (red) mice. In Emx1-cKO*
258 *samples, less signal expression is seen in the most anterior regions (ACC and M2, but not M1), whereas*
259 *increased signal is quantified in parietal and occipital regions (S1, A, V. and RSC), relative to the control*

*condition. In Nex-cKO animals, the amount of signal is reduced in ACC, M2 and M1, with no statistical difference in S1 compared to controls, but with increased amount of signal in A, V, and RSC, even if lower than in Emx1-cKOs. * < 0.05, **< 0.01, ***<0.005, #<0.0001. Data are represented as mean ± SEM. Data were analyzed with 2way-ANOVA test and corrected for multiple comparison with the Bonferroni test (see also **Supplementary Table 4**). Ctrl, n=6; Emx1-cKO, n=4, Nex-cKO, n=4. Abbreviations: A, auditory cortex; ACC, anterior cingulate cortex; CA1, cornu ammonis area 1; CB, cerebellum; CP, cerebral peduncle; CST, corticospinal tract; Cx, cortex; fi, fimbria; GC, gustatory cortex; LFP, longitudinal fascicle of the pons; M1, primary motor cortex; M2, secondary motor cortex; MB, mammillary body; OB, olfactory bulb; PFC, prefrontal cortex; PN, pontine nuclei; RSC, retrosplenial cortex; S1, primary somatosensory cortex; SC, superior colliculus; Sb, subiculum; Th, thalamus; V, visual cortex. Scale bars, 1mm (**A**); 500µm (**B-D; B'-D'**).*

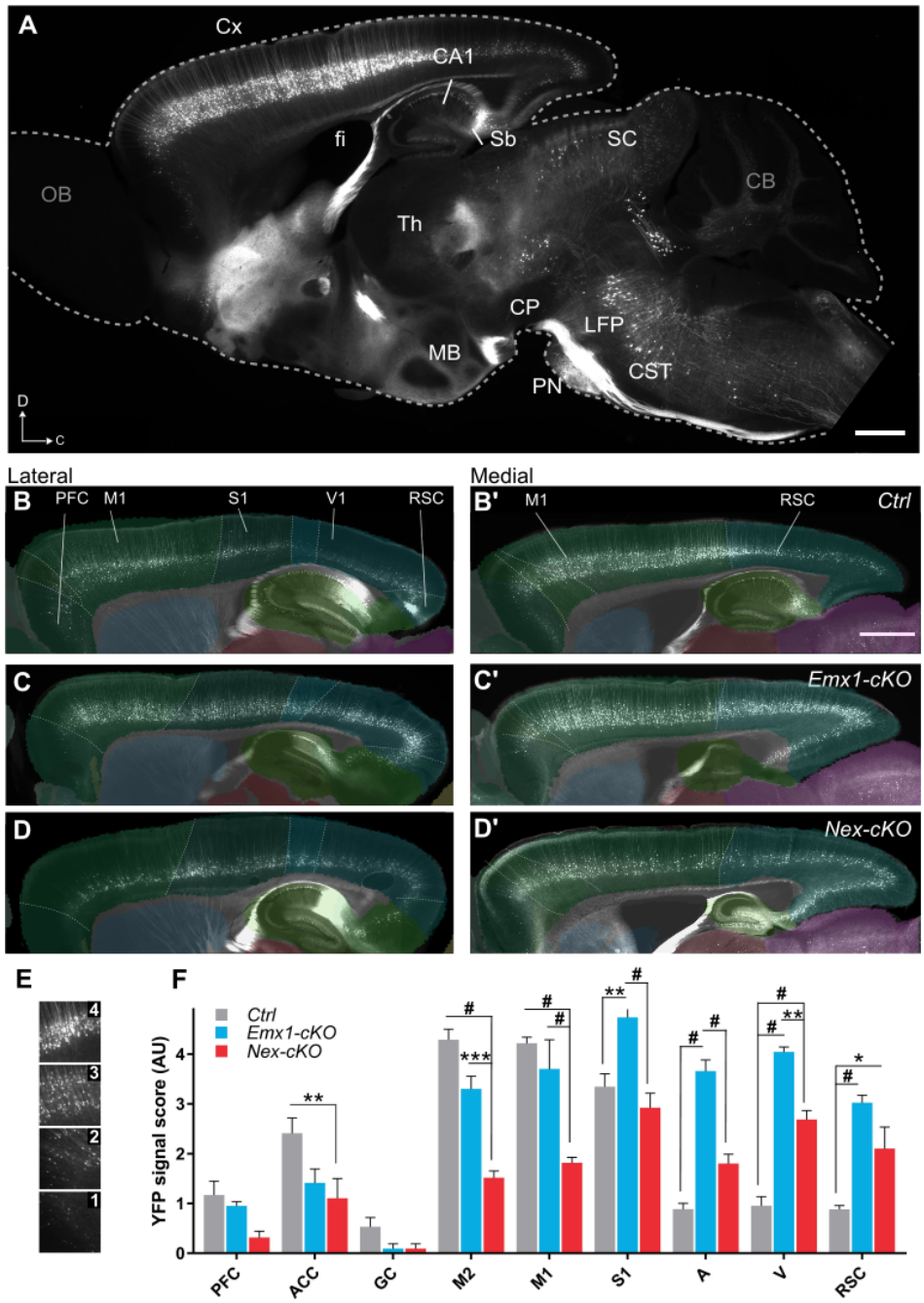

273 **Abnormal corticospinal projections and fasciculation in *Nr2f1* mutant brains**

274 We hypothesized that the disordered cortical distribution of YFP-expressing layer V neurons
275 in mutant mice might influence the integrity of subcortical axonal projections. In all cases
276 (mutant and controls alike), strong YFP signal expression was seen bilaterally in the main
277 corticofugal pathways (**Figure 3A)**, visible as longitudinally oriented fiber bundles coursing
278 through the caudoputamen towards the cerebral peduncle (**Figure 4A-D)**, passing dorsal to
279 the pontine nuclei as the longitudinal fasciculus of the pons (**Figure 4B'-D')**, and continuing
280 through the brain stem towards the spinal cord as the CST. Since a large fraction of the
281 corticobulbar fibers terminate in the pontine nuclei (Tomasch, 1968; Tomasch, 1969), we
282 reasoned that abnormal distribution of YFP-expressing layer V neurons observed in mutant
283 mice (**Figure 3**) might affect corticopontine innervation, and could be reflected in an abnormal
284 size of the pontine longitudinal fascicle as it enters the cerebral peduncle and exits the pons
285 in rostral and caudal positions to the pontine nuclei, respectively. To evaluate this, we
286 measured the dorsoventral width of the longitudinal fascicle of the pons in sequential sections
287 along the medio-lateral axis. The measurements were taken at rostral and caudal levels to the
288 pontine nuclei in the three genotypes (**Figure 4A'**). Surprisingly, we found the lateral part of
289 the fascicle to be wider at both rostral and caudal levels in *Nex-cKO* mice compared to *Emx1-*
290 *cKO* and controls, while being narrower medially (see red area chart in **Figure 4E, F**). This
291 suggests that the longitudinal fascicle of the pons is flattened and expanded laterally upon
292 Nr2f1 inactivation in postmitotic neurons. Smaller differences were observed in the *Emx1-*
293 *cKO* fascicle which shape was however more similar to controls than to the *Nex-cKO* one (blue
294 area chart in **Figure 4E, F**). This is also supported by quantification of the total surface of the
295 longitudinal fascicle of the pons at rostral and caudal levels, which shows a significant surface
296 reduction at caudal but only a tendency at rostral levels in *Emx1-cKO* mice (**Figure 4G, H**).
297 These data indicate that loss of Nr2f1 in progenitors, but not in neurons, results in fewer YFP-
298 expressing fibers passing the pontine nuclei towards the brain stem to form the CST.

299 Moreover, we observed, caudal to the pontine nuclei, abnormally widespread fiber fascicles
300 in the CST of mutant animals (arrowheads in **Figure 4C', D'**). To determine whether this was
301 a significant difference between animal groups, we estimated the degree of fiber bundle
302 fasciculation in the CST of *Emx1-cKO* and *Nex-cKO* mice. At locations of 250μm and 500μm

303 caudal to the pontine nuclei (**Figure 4A'**), we measured the total dorsoventral width of the
304 CST at several mediolateral levels and subtracted the width of gaps between the YFP-
305 expressing fiber bundles at the same levels. The ratio of the total width of the CST and width
306 of the fibers only was used as a measure of the fasciculation index **(Figure 4I**). Notably, in both
307 groups of mutant mice, we found a lower degree of fasciculation in the CST which was more
308 pronounced at the most caudal level (**Figure 4I**). Together, these data show that loss of *Nr2f1*
309 expression (both in cortical progenitor cells and postmitotic cells) affects the diameter, shape
310 and degree of fasciculation of the CST originating from layer V neurons.

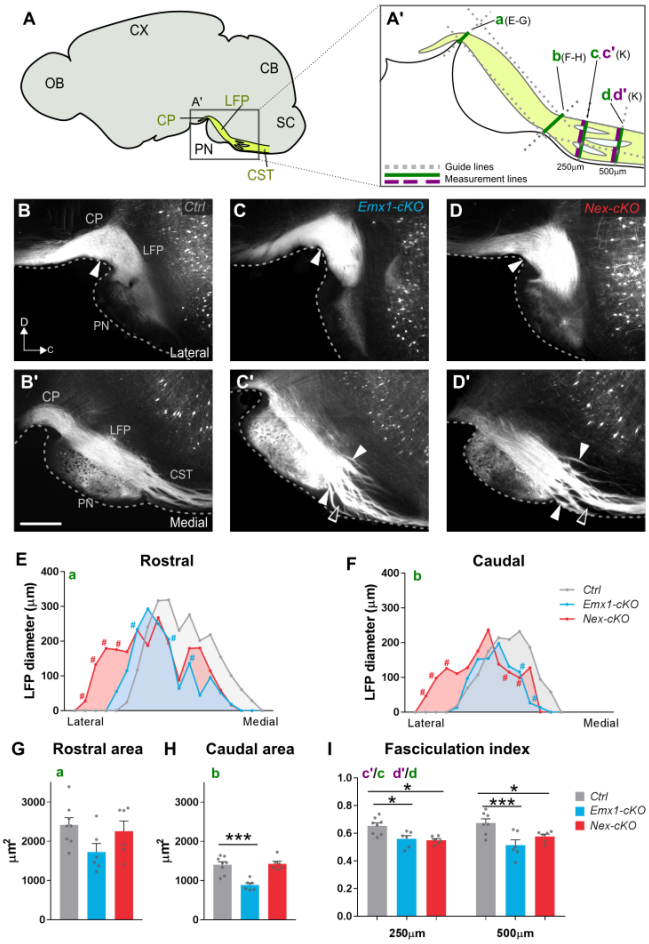

311

312 ***Figure 4 – Loss of Nr2f1 function leads to abnormal corticospinal projections and fasciculation.*** *(**A**)*
313 *Schematic diagram of a sagittal mouse brain section showing the location of the pontine nuclei (PN) and*
314 *descending fiber tracts (yellow) in the cerebral peduncle (CP), longitudinal fascicle of the pons (LFP) and*
315 *corticospinal tract (CST) at level of the pons. (**A'**) Diagram taken from A illustrating the different*
316 *measurements shown in E-I. The frame reflects the region shown in **B-D** and **B'-D'** in control (Ctrl), Emx1-*
317 *cKO and Nex-cKO animals. (**B-D**) Lateral sagittal section showing the corticospinal tract entering the pons*
318 *level as a continuation of the cerebral peduncle. White arrowheads point to the site of measurement plotted*
319 *in E, showing a similar thickness of the bundle in the three genotypes. (**B'-D'**) Medial sagittal section*
320 *showing the corticospinal tract passing dorsal to the pontine nuclei and defasciculating prior to entering*

321 *the spinal cord. Full arrowheads point to fiber bundles (thinner and more dispersed in both Emx1-cKO and*
322 *Nex-cKO mutants), empty arrowheads point to empty spaces between bundles. (**E, F**) Plots showing LFP*
323 *diameter measurements obtained from lateral to medial before and after innervating the pontine nuclei*
324 *(rostral and caudal respectively) for the three genotypes. Each measurement represents the average value*
325 *of corresponding sections among distinct animals and each position on the x-axis represents a specific*
326 *section of the series. (**G-H**) Column graphs showing average values of the area under the curves in **E-F**. A*
327 *comparable number of fibers reach the cerebral peduncle in the three genotypes (**G**). In Emx1-cKO brains*
328 *fewer fibers are seen to exit the level of the pons compared to control- and Nex-cKO brains (**H**). (**I**) Column*
329 *graph showing CST fasciculation index, based on measurements of total thickness and fiber thickness (green*
330 *and purple line respectively in **A'**) performed at 250 and 500 µm from the terminal edge of the pontine*
331 *nuclei. A ratio between the two measurements was calculated for each position. Data are represented as*
332 *mean ± SEM. Data were analyzed with 2way-ANOVA test (**E-F**) or ordinary one-way ANOVA test (**G-I**) and*
333 *corrected for multiple comparison with the Bonferroni test (see also Supplementary Table 4). Ctrl, n=8;*
334 *Emx1-cKO, n=6; Nex-cKO, n=6. #<0.05 (**E-F**) * < 0.05, **< 0.01, ***<0.005 (**G-I**). Abbreviations: CB,*
335 *cerebellum; CP, cerebral peduncle; CST, corticospinal tract; CX, cortex; LFP, longitudinal fascicle of the pons;*
336 *OB, olfactory bulb; PN, pontine nuclei; SC, spinal cord. Scale bar, 500µm (**B'**).*

337

338 **Dual role of Nr2f1 in targeting corticopontine projections**

339 Next, we evaluated whether topographical organization of corticopontine projections was
340 dependent on proper cortical area mapping and layer V distribution (**Figure 5**). To this
341 purpose, we assessed the spatial distribution of YFP signal expression within the pontine
342 nuclei by comparing intensity-normalized microscopic images of spatially corresponding
343 sagittal sections from the brains of *Emx1-cKO*, *Nex-cKO* and control littermate animals (**Figure**
344 **1**B; **Figure 5A**). In all mice, widespread signal expression was seen across most parts of the
345 pontine nuclei (**Figure 5B-L**). A complete documentation of spatially comparable and
346 reproducible images showing YFP expression in the pontine nuclei of all mutant mice and
347 controls is provided in **Supplementary Figures 1 and 2**. In control brains, we observed a strong
348 YFP signal in central parts of the pontine nuclei, with the densest expression tending to
349 surround a centrally located zone exhibiting less dense signals (**Figure 5B-E**). This region of
350 the pontine nuclei typically receives strong projections from S1 areas (green dots in **Figure**
351 **2G-K**). Some signal expression was also visible in medial parts of the pontine nuclei (**Figure**
352 **5D, E**), which is known to primarily receive projections from the cortical motor areas (purple
353 dots in **Figure 2G-K**). By contrast, signal expression was lower in rostral and lateral parts of
354 the pontine nuclei (**Figure 5B, C, E**), which are known to receive projections from visual and
355 auditory areas of the cerebral cortex (Inoue et al., 1991; Leergaard and Bjaalie, 2007).

356 Interestingly, *Emx1-cKO* mice showed a relatively homogeneous signal distribution across all
357 parts of the pontine nuclei, and notably also displayed more signal expression in the
358 dorsolateral regions (**Figure 5F-I**). Signal expression was also present in the medial part of the
359 nuclei (**Figure 5G-I**). This observation fits well with the finding of more extensive YFP signal
360 expression in the occipital cortex (**Figure 3C,C'**), which projects to the dorsolateral pontine
361 nuclei. By comparison, the signal expression observed in *Nex-cKO* animals was more
362 constrained and predominated in rostrally and caudally located clusters extending from the
363 cerebral peduncle towards the ventral surface of the pons, and medially surrounding a central
364 core in which little signal was expressed (**Figure 5J-M**). These clusters were more peripherally
365 located than the clustered signal expression observed in control animals (**Figure 5J-M**).
366 Notably, in all *Nex-cKO* cases little signal expression was seen in the central region of the PN
367 (unfilled arrowheads in **Figure 5J-L**), despite the presence of YFP-expressing layer V neurons
368 in S1 (**Figure 3D,D', F**). This central region is normally innervated by projections from the face
369 representations located in S1 (**Figure 2A-F**).

370 Taken together, these findings show that corticopontine projections are abnormally
371 distributed in *Nr2f1* cortical deficient mice, with more homogenously (non-specific)
372 distributed expression in *Emx1-cKO* mice (schematically summarized in **Figure 5N,0**), and
373 more peripherally distributed signal expression in *Nex-cKO* mice, that display reduced
374 expression in the central region of the pontine nuclei normally receiving S1 projections
375 (schematically summarized in **Figure 5N,P**). In both mutant groups the signal expression was
376 expanded to dorsolateral regions of the pontine nuclei that normally are innervated by
377 projections from occipital cortical areas. This suggests that cortical Nr2f1 graded expression
378 in postmitotic neurons might be directly involved in the establishment of topographically
379 organized corticopontine projections.

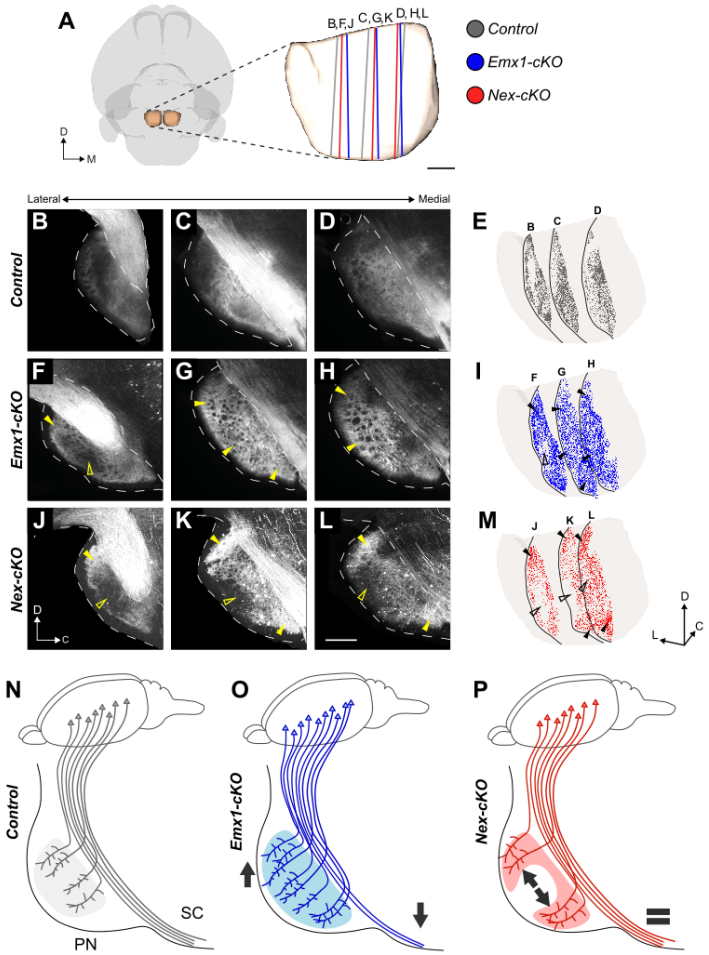

Figure 5 - Distribution of YFP signal expression in the pontine nuclei in knock-out mice and controls. *(**A**) 3D representation of the outer surfaces of the brain (transparent grey) and pontine nuclei (transparent brown) from the Allen mouse brain atlas. Pontine nuclei enlarged in ventral view with colored lines representing the location and orientation of the sagittal sections shown in **B-M**. (**B-D, F-H, J-L**) Fluorescence microscopy images of sagittal sections from corresponding mediolateral levels of the pontine nuclei, showing the spatial distribution of YFP signal expression in control, Emx1-cKO, and Nex-cKO mice, respectively. (**E, I, M**) 3D visualization of the transparent external surface of the pontine nuclei in an oblique view from ventromedial, with point coded representations of signal expression from the sagittal sections shown in **B-D**, **F-H**, and **J-L**, respectively. Filled yellow or black arrowheads point to regions with increased signal expression in mutant mice, while non-filled arrowheads indicate regions with decreased signal expression. In control mice (**B-E**), signal expression is primarily seen in central and caudal parts of the pontine nuclei, while in Emx1-cKO mice (**F-I**) signal expression is more widespread and diffuse throughout the entire pontine nuclei, including more peripheral parts of the pontine nuclei towards rostral, ventral and caudal positions (filled arrowheads in **G-I**). In Nex-cKO mice (**J-M**), signal expression is reduced in the central core region of the pontine nuclei (non-filled arrowheads in **K-M**), while being increased in peripheral (rostral and caudal) regions of the pontine nuclei. (**N-P**) Diagrams summarizing observed changes in corticopontine connectivity upon Nr2f1 inactivation. In control mice (**N**), YFP⁺ corticopontine projections primarily target central part of the PN and a substantial amount of fibres continue towards the spinal cord. In Nr2f1 Emx1-cKO mutants (**O**), fewer fibres reach the SC and more projections target the PN (down- and up-pointing grey arrows, respectively) and show a pattern of innervation more diffused and widespread that in controls. Finally, in Nr2f1 Nex-cKO animals (**P**), no difference between corticospinal and corticopontine projections are detected compared to controls (grey equal sign), but corticopontine topography appears to be affected, whereby fibres reach more lateral, motor-receiving PN regions instead of targeting the S1-receiving core (illustrated by grey divergent arrows). Abbreviations: C, caudal; D, dorsal; L, lateral; M, medial, PN, pontine nuclei; R, rostral; SC, spinal cord. Scale bar, 200 µm.*

406 **Altered somatosensory topographic projections in *Nex-cKO* adult mutant mice**

407 Our data thus show that loss of Nr2f1 function in progenitors (*Emx1-cKO*) results in aberrant
408 and homogenous corticopontine projections, whereas loss of Nr2f1 in neurons (*Nex-cKO*)
409 display a peripherally-shifted innervation pattern (**Figure 5N-P**). To further support that *Nr2f1*
410 gradient cortical expression might be directly involved in topographical pontine mapping, we
411 decided to focus on the *Nex-cKO* genetic model and unveil the cortical origin of the
412 innervation defect. Compared to the *Emx1-cKO* mice, in which projections are more diffuse
413 and abundant, we considered the *Nex-cKO* mouse model more suitable for investigating the
414 changes in topographical mapping in more detail using experimental tract tracing techniques.
415 We therefore injected the AAV9-CAGtdTomato anterograde viral tracer (Pourchet et al.,
416 2021) in motor, lateral or medial S1 cortex of 5 days-old (P5) *Nex-cKO* mice and littermate
417 controls (**Figures 6, 7**). The mice were sacrificed at P21 and brain sections analyzed
418 microscopically (**Figure 1B)**. All histological sections were spatially registered to the *Allen*
419 *Mouse Brain Atlas* (common coordinate framework, CCF3; (Wang et al., 2020)), and the
420 location of tracer injections sites were mapped in the same atlas space (**Figures 6A, 7A**). For
421 each injection site location in a *Nex-cKO* brain, we selected either the most corresponding
422 control experiment or wild-type tract-tracing data from the *Allen Mouse Brain Connectivity*
423 *Atlas*, as additional controls. Representative examples of injections and comparisons between
424 controls and littermate *Nex-cKO* brains are shown in **Figures 6B-C' and 7B-C'**. *Complete*
425 *documentation of all tracing experiments cases is provided in* ***Supplementary Figure 3*** *(TO BE*
426 *COMPLETED WITH THE NEXT REVISION OF THE MANUSCRIPT).*

427 In all control mice, the spatial distributions of corticopontine projections (dark gray point
428 clouds in **Figures 6 and 7**) were comparable with the labelling patterns seen in corresponding
429 wild-type tracing data from the *Allen Mouse Brain Connectivity Atlas*. As expected, tracer
430 injections into motor areas gave rise to labelled axonal clusters located rostrally, caudally, and
431 medially in the pontine nuclei (purple dots in **Figure 2G-K**, **Figure 6D-F**). In all *Nex-cKO* mice
432 receiving tracer injections into cortical motor areas, the overall distribution of corticopontine
433 labeling was found to be essentially similar to that observed in the control cases (compare
434 grey point with red point clouds in **Figure 6D-F**).

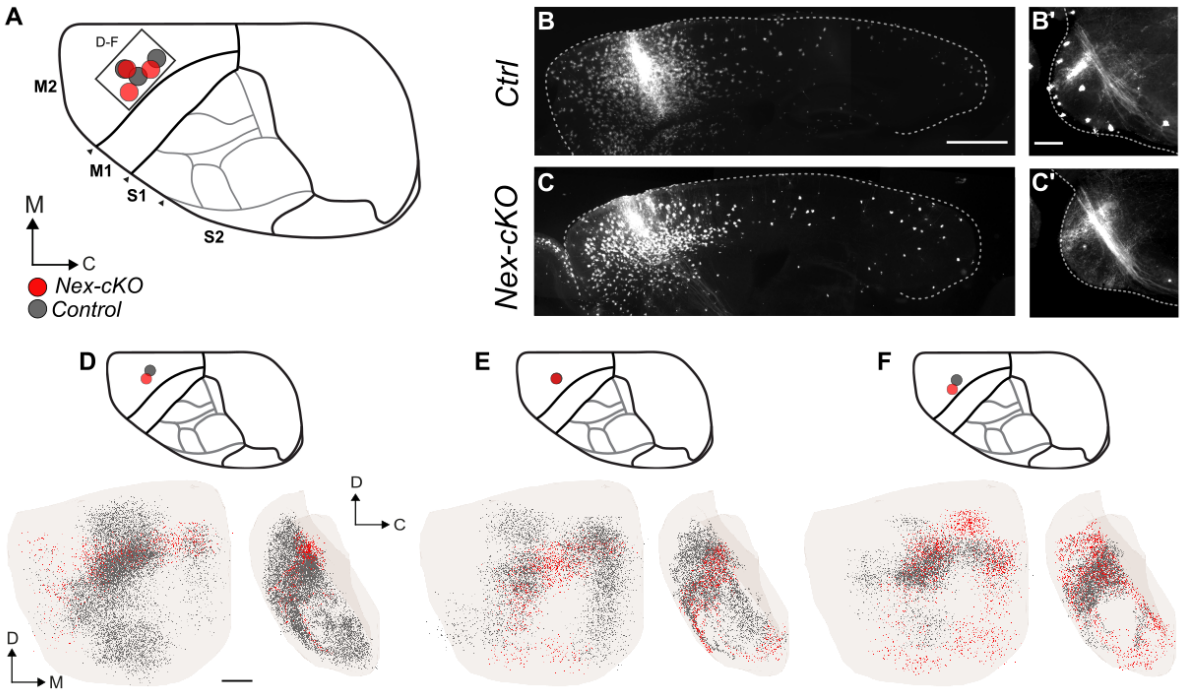

435

436 ***Figure 6. Anterograde tracing of corticopontine projections from motor areas in Nex-cKO mice.*** *(**A**)*
437 *Overview of the location of the anterograde viral tracer injection sites in the right primary (M1) and*
438 *secondary motor cortex (M2) in Nex-cKO (red) and control (dark grey) brains. (**B, B'** and **C, C'**) representative*
439 *macroscopic images of the injection site localization (**B-C**) and pontine nuclei innervation (**B', C'**) in the*
440 *control and Nex-cKO cases reported in panel **F**. (**D-F**) 3D coloured point clouds representing axonal labelling*
441 *in corresponding pairs of Nex-cKO (red) or control/wild-type (dark grey) mice, shown within a transparent*
442 *surface representation of the right pontine nuclei in ventral and medial views. Inset drawings of the brains*
443 *seen from dorsal show the location of tracer injection sites for each combination of point clouds. Tracer*
444 *injections in corresponding locations in M2 of both Nex-cKO and control/wild-type mice give rise to similar*
445 *corticopontine labelling in rostrally located clusters, curving towards ventral and caudal along the surface*
446 *of the pontine nuclei. Abbreviations: C, caudal; D, dorsal; M, medial; M1, primary motor cortex; M2,*
447 *secondary motor cortex; S1, primary somatosensory cortex; S2, secondary somatosensory cortex. Scale*
448 *bars, 1mm (**B**) 200 µm (**B',D**).*

449 Tracer injections into S1 areas of control animals gave rise to labelled axonal clusters located
450 centrally and caudally in the pontine nuclei (grey point clouds in **Figure 7D-I**). By contrast,
451 tracer injections into S1 representations of the whiskers or upper limb, or into the S1/M1
452 (sensorimotor) lower limb representation in *Nex-cKO* brains gave rise to abnormal
453 distribution of corticopontine fibers (**Figure 7D-G**). Specifically, while the S1 corticopontine
454 projections in wild-type mice typically form a large, elongated, caudally or laterally located
455 cluster (**Figure 7D-F**, dark grey points), this labelling was shifted towards more rostral
456 locations in the *Nex-cKO* brains (**Figure 7D-F**, red points), resembling the distributions
457 observed after tracer injections into motor areas (**Figure 6D-F**).

458 Notably, tracer injections placed in the anterolateral part of S1 in *Nex-cKO* mice, in regions
459 representing sensory surfaces of the head, gave rise to labelled axons distributed in the
460 central part of the pontine nuclei, with more subtle difference to the matching control
461 experiments (**Figure 7G)**. In two cases, projections from the S1 head region were distinctly
462 shifted towards medial relative to a control experiments (red dots in **Figure 7G, and I**),
463 attaining a distribution resembling the corticopontine projections from head representations
464 in M1 cortex, located significantly more anteriorly in the cortex (gray dots in **Figure 7I**). These
465 results indicate that corticopontine projections from the head representations of S1 also
466 display abnormal topographical distributions resembling the normal projections from
467 homologous representations in the primary motor cortex. Finally, one tracer injection placed
468 in the most anterolateral part of S1, representing perioral surfaces in a *Nex-cKO* mouse,
469 yielded corticopontine labelling which was highly similar to that of a control experiment
470 (**Figure 7H**). This finding of normal projection topography from this early generated part of
471 the cortex, may be explained by the late Nr2f1 genetic inactivation, which occurs after the
472 earliest layer V neurons have been produced.

473 Our findings thus show that corticopontine projections from motor areas and the most
474 anterolaterally located parts of S1 are topographically similar in *Nex-cKO* brains and controls,
475 whereas corticopontine projections from most parts of S1 (head, whisker, upper limb, and
476 lower limb representations) are abnormally shifted towards rostral and medial regions of the
477 pontine nuclei, that normally receive projections from cortical motor areas (schematically
478 summarized in Fig. 7J,K). This is in overall agreement with the spatial and temporal control of
479 Nr2f1 in area mapping. Indeed, no changes in motor-deriving corticopontine projections
480 might be due to low Nr2f1 expression in rostral/motor cortex (spatial control), whereas no
481 changes in the projections originating from the most anterolateral part of S1, the earliest
482 cortical projections to innervate the forming pontine nuclei, might be explained by the late
483 Nr2f1 genetic inactivation occurring after the earliest layer V neurons have been produced
484 (temporal control).
485

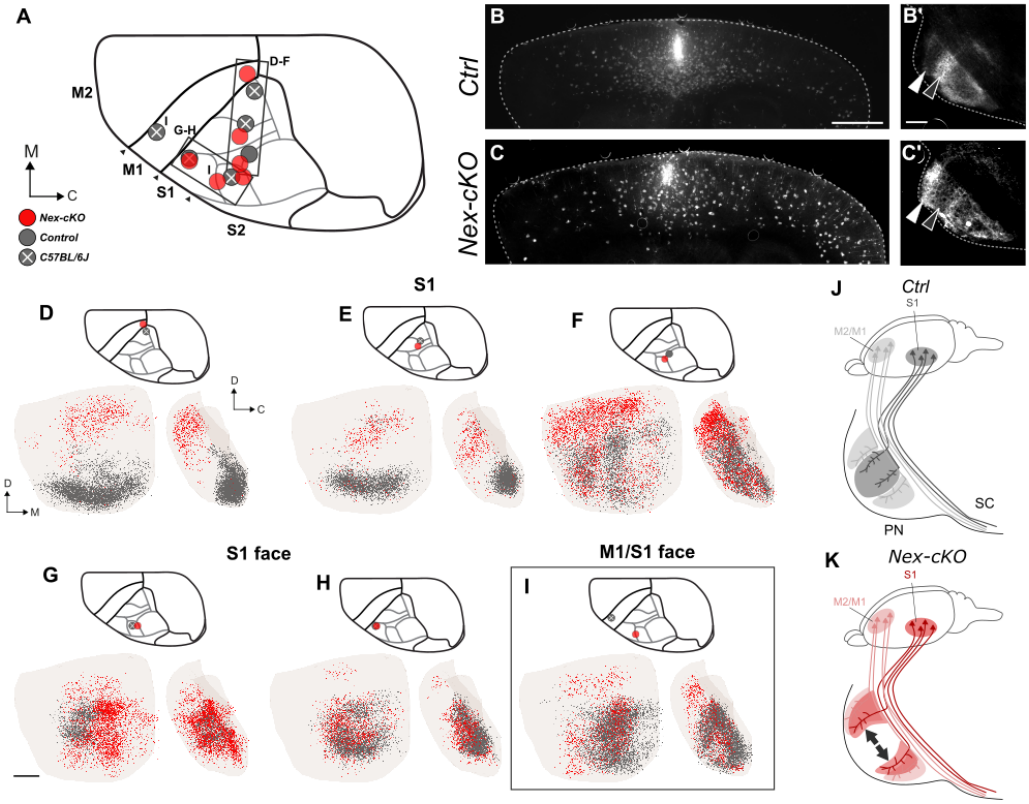

Figure 7. Anterograde tracing of corticopontine projections from somatosensory areas in Nex-cKO mice. *(**A**) Overview of the location of the anterograde viral tracer injection sites in the right primary somatosensory (S1) cortex in Nex-cKO (red), control (dark grey), and wild-type C57BL/6J (dark grey with white cross, data from the Allen Mouse Brain Connectivity Atlas) brains. (**B, B'** and **C, C'**) representative macroscopic images of the injection site localization (**B-C**) and pontine nuclei innervation (**B', C'**) in the control and Nex-cKO cases reported in panel **F**. (**D-I**) 3D coloured point clouds representing axonal labelling in corresponding pairs of Nex-cKO (red) or control/wild-type (dark grey) mice, shown within a transparent surface representation of the right pontine nuclei in ventral and medial views. Inset drawings of the brains seen from dorsal show the location of tracer injection sites for each combination of point clouds. Corresponding tracer injections in lower limb and upper limb representing regions in S1 of Nex-cKO and control/wild-type mice give rise to labelling in different parts of the pontine nuclei, with corticopontine projections in control mice distributed in elongated curved clusters located caudally (grey points in **D,E**) or laterally in the pontine nuclei (grey points in **F**), while projections from the same locations in Nex-cKO mice are shifted to more peripheral rostral and lateral parts of the pontine nuclei (red points in **D-F**). All tracer injections in the face region of Nex-cKO and control mice gave rise to labelling in the central region of the pontine nuclei, however with a subtle medial shift of projections in Nex-cKO brains (**G**, see also **I**). Corresponding tracer injections in the most anterolateral part of S1 in a Nex-cKO and wild-type control gave rise to highly similar labelling, centrally in the pontine nuclei. (**I**) Tracer injections in widely separated locations in S1 (Nex-cKO) and M1 (wild-type control) gave rise to largely corresponding labelling in the medial part of the central core region of the pontine nuclei, albeit with additional rostral and medial labelling in the Nex-cKO experiment. This demonstrates that corticopontine projections from S1 in Nex-cKO mice are changed to resemble normal projections from M2. (**J-K**) Diagrams summarizing observed changes in corticopontine connectivity upon Nr2f1 postmitotic inactivation. In control mice (**J**), projections from motor areas (M2/M1, pink) and S1 (purple) target largely segregated parts of the pontine nuclei, with somatosensory projections targeting the central core region, while motor projections target more peripheral rostral, caudal, and medial parts of the pontine nuclei. In Nr2f1 Nex-cKO animals, corticopontine topography of S1 is affected, whereby fibres reach lateral, motor-receiving PN regions instead of targeting the core (illustrated by grey divergent arrows). Abbreviations: C, caudal; D, dorsal; M, medial; M1, primary motor cortex; M2, secondary motor cortex; PN, pontine nuclei; S1, primary somatosensory cortex; S2, secondary somatosensory cortex, SC, spinal cord. Scale bars, 1mm (**B**), 200 µm (**G**).*

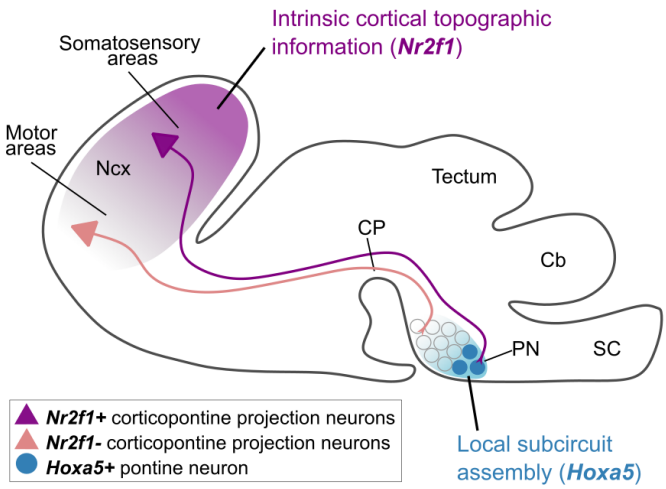

Figure 8. Model of corticopontine topography establishment. *Proposed schematic model of how the neocortex (Ncx) and the pontine nuclei (PN) might interact during development in driving corticopontine topography. Both structures need to be pre-patterned by gradient expression of transcription factors. While postmitotic pontine graded expression of Hoxa5 will impart an anterior to posterior identity to pontine neurons (graded blue circles) (Maheshwari et al., 2020), postmitotic cortical gradient expression of Nr2f1 (purple gradient in Ncx) will intrinsically instruct corticopontine neurons (dark and light purple tracts) to innervate their topographically proper targets (this study). Abbreviations: Cb, cerebellum; CP, cerebral peduncle; SC, spinal cord.*

DISCUSSION

Our present study questions whether and how spatio-temporal cortical expression gradients are involved in the establishment of normal topographical organization of corticopontine projections. By combining genetically modified mice and public mouse brain connectivity data with tract-tracing techniques and digital brain atlas tools, we have provided novel evidence of an intrinsic molecular control of layer V cortical neurons during the establishment of topographical organization of corticopontine projections in a spatial and temporal fashion. Abnormal areal organization in the neocortex induced by Nr2f1 inactivation is reflected in altered corticopontine projections, as well as impaired structural integrity of the CST. While loss of *Nr2f1* from the early progenitor cell pool leads to increased and abnormal corticopontine innervation at the expense of corticospinal projections, only late postmitotic *Nr2f1* inactivation reveals altered topographic pontine mapping from medially located parts

540 of somatosensory cortex controlling whisker, upper limb, and lower limb representations. No
541 shifts from motor and somatosensory anterolateral projections were observed in these mice,
542 in line with a spatial and temporal control of Nr2f1 expression, respectively. Overall, our data
543 show that proper area mapping of the neocortical primordium is a pre-requisite for preserving
544 the cortical spatial and temporal segregation within the pontine nuclei, and thus correct
545 corticopontine topographic organization.

546

547 **Spatial accuracy of topographical data compared across experiments**

548 To ensure proper accuracy of 3D data in wild-type and genetically-modified mice, we relied
549 on spatial alignment of serial microscopic section images to a common atlas reference space,
550 achieved through a two-step atlas registration method (Puchades et al., 2019), which included
551 adjustment of section orientation and non-linear refinement. The process allowed us to
552 record and compare axonal projections as 3D data points in an interactive viewer tool. The
553 use of non-linear registration compensated for minor shape differences among brains and
554 allowed comparison of distribution patterns among spatially relevant data. The focus on the
555 location rather than the amount of signal expression/axonal labelling also compensated for
556 the variation in signal expression intensity and size of tracer injections among cases. The
557 approach to comparing axonal distributions as semi-quantitatively recorded data points in 3D
558 was adopted from well-established methods used in earlier studies of cerebro-cerebellar
559 organization in rats (Leergaard et al., 2000a; Leergaard and Bjaalie, 1995; Leergaard et al.,
560 1995; Leergaard et al., 2000b; Lillehaug et al., 2002). By representing signal expression and
561 axonal labeling as 3D point clouds, it became possible to more directly explore and compare
562 location and distribution patterns in 3D in different combinations of data sets. For the
563 additional benchmark data extracted from the *Allen Mouse Brain Connectivity Atlas*, we used
564 the same sagittal image orientation as in our microscopic data, to facilitate comparison of
565 microscopic images in addition to the 3D comparisons. The relevance and accuracy of the
566 approach was confirmed by demonstrating that similarly located cortical tracer injections in
567 control animals gave rise to similarly distributed labelling patterns in the pontine nuclei.

568

569

570 **Mitotic versus postmitotic Nr2f1 functions in layer V corticofugal projections**

571 Our previous work has shown overall areal organization impairments in both *Nr2f1* mutant
572 brains, independently of whether Nr2f1 was inactivated in progenitors or postmitotic
573 neurons. However, gain-of-function experiments demonstrated that sensory area identity
574 was mainly controlled by Nr2f1 expression in postmitotic cells, showing that early
575 differentiating neurons acquire proper sensory identity only after progenitors leave the cell
576 cycle (Alfano et al., 2014b). Here, we report for the first time that Nr2f1 drives corticopontine
577 connectivity differently in progenitors *versus* postmitotic neurons. While Nr2f1 expressed by
578 progenitor cells modulates the ratio between corticopontine and corticospinal axonal
579 projections, similarly to what happens in *C. elegans* with the ortholog UNC-55 (Petersen et
580 al., 2011; Zhou and Walthall, 1998), postmitotic Nr2f1 expression specifically acts on S1
581 topographic organization of corticopontine neurons (**Figures 4, 5**). This suggests that early
582 Nr2f1 expression in progenitor cells is mainly required in the specification and most probably
583 axonal guidance of layer V subtypes, while later postmitotic expression is more implicated in
584 the refinement of corticopontine topographical organization. Interestingly, the altered
585 distribution of layer V YFP expression observed in the *Emx1-* and *Nex-cKO* cortex relative to
586 control animals, correspond well with the differences in pontine innervation. A higher
587 production of layer V neurons in S1 of *Emx1-cKO* mice leads to increased corticopontine
588 innervation, in accordance with increased Lmo4 expression, known to drive layer V neurons
589 versus the pontine nuclei (Cederquist et al., 2013; Harb et al., 2016). Differently, the *Nex-cKO*
590 S1 cortex maintains a similar number of YFP layer V neurons, but their axons project to
591 pontine targets normally innervated by motor-derived cortical areas. Finally, increased signal
592 expression in visual and auditory areas in the occipital cortex, corresponds with an increased
593 innervation in dorsolateral regions of pontine nuclei known to receive projections from the
594 occipital cortex. These data well illustrate a dual role for Nr2f1 in layer V corticofugal
595 connectivity, an early one in subtype specification (corticopontine vs corticospinal), and a
596 later one in topographical mapping.

597

598 **Revising the chrono-architectonic hypothesis of cortico-pontine circuit development**

599 Previous data in developing rats have shown that pontine neurons settle in the forming
600 pontine nuclei in a shell-like fashion according to their birthdate with early born neurons
601 forming the central core of the pontine nuclei and later born neurons consecutively settling

602 around the earlier born neurons forming concentric rings (Altman and Bayer, 1987). In
603 parallel, at early postnatal stages, corticopontine axons are chemotropically attracted as
604 collateral branches from corticospinal axons (Heffner et al., 1990; O'Leary and Terashima,
605 1988), and innervate the pontine nuclei in a topographic inside-out pattern (Leergaard et al.,
606 1995), which is further refined through adult stages (Leergaard and Bjaalie, 2007). Neurons in
607 the frontal (motor) cortex project rostrally and medially in the pontine nuclei, neurons in the
608 parietal (somatosensory) cortex project to central and caudal parts, neurons in the temporal
609 (auditory) cortex to central and lateral regions, and neurons in the occipital (visual) cortex to
610 lateral and rostral parts of the pontine nuclei (Leergaard and Bjaalie, 2007). This concentric
611 organization of corticopontine projections suggests that the birthdate of pontine neurons and
612 the inside-out genesis of the pontine nuclei is linked to the spatial organization of cortical
613 inputs.
614 However, intrinsic differences in pontine neurons born at different times might also have an
615 instructive role for corticopontine innervation. A recent study in mice showed that
616 postmitotic expression of the HOX gene *Hoxa5* guides pontine neurons to settle caudally
617 within the pontine nuclei, where they are targeted by projections from limb representations
618 in the somatosensory cortex (Maheshwari et al., 2020). Moreover, ectopic Hoxa5 expression
619 in pontine neurons is sufficient to attract cortical somatosensory inputs, regardless of their
620 spatial position in the pontine nuclei, showing that pontine neurons can play an instructive
621 and attractive role in topographic input connectivity of corticopontine neurons (Maheshwari
622 et al., 2020).

623 Nevertheless, maturational gradients in the pontine nuclei cannot fully explain the complexity
624 of the fine-grained somatotopic topographic connectivity pattern between cortical input and
625 pontine neuron targets. Since the establishment of topographic maps requires multiple
626 processes and structures, it is conceivable that the position and specific intrinsic molecular
627 programs of both presynaptic afferents and postsynaptic target neurons contribute to this
628 complex corticopontine connectivity map. Indeed, our data show that without affecting the
629 development and maturation of pontine neurons, corticopontine Nr2f1-deficient layer V
630 axons originating from S1 areas in the parietal cortex will abnormally target the pontine
631 region normally deputed to corticopontine motor axons. By contrast, Nr2f1-deficient axons
632 originating from the frontal and medial cortex will innervate the expected pontine region

allocated to motor axons. This strongly suggests that during the establishment of corticopontine topography, both structures, the neocortex and the pons need to be properly pre-patterned by factors involved in spatial and temporal control of neurogenesis, such as Nr2f1 for the cortex, and Hoxa5 for the pontine nuclei (schematically summarized in **Figure 8**).

Conclusion and outlook

With the present study, we have provided new insights into the developmental mechanisms establishing topographical organization by showing that gradient cortical expressions of transcription factors, in this case Nr2f1, are directly involved in the establishment of corticopontine topographic mapping. However, it is likely that other factors regulating area size and positions might also be implicated in the same process. We conclude that distinct molecular mechanisms in the source (cerebral cortex) and target (pontine nuclei) regions must be coordinated during the establishment of corticopontine topography. Identifying the molecular pathways within the cortex and pontine nuclei, as well as the mechanisms and molecules governing their interaction remains an open question for further studies.

ACKNOWLEDGEMENTS

We thank Isabelle Dusart in Paris for providing us with AAV9-CAG-tdTomato viral particles produced by Alexis Bemelmans (CEA, France), Nicolaas Groeneboom and Gergely Csucs for expert technical assistance, the iBV PRISM platform for imaging and automatic quantification support, and Sharon Yates, and Maja A. Puchades for useful discussions. This work was funded by the "Fondation Recherche Médicale; Equipe FRM 2015" #DEQ20150331750 to M.S.; by an ''Investments for the Future'' LabEx SIGNALIFE (grant ANR-11- LABX-0028-01) to M.S., by a PhD contract from Région PACA/Inserm and FRM 4th year PhD for C.T, with additional funding from the European Union's Horizon 2020 Framework Program for Research and Innovation under the Specific Grant Agreement No. 785907 (Human Brain Project SGA2), Specific Grant Agreement No. 945539 (Human Brain Project SGA3), and The Research Council of Norway under Grant Agreement No. 269774 (INCF Norwegian Node) to JGB and TBL.

Competing interests: The authors declare no financial and non-financial competing interests.

663 **MATERIALS AND METHODS**

664 **Topographical map of corticopontine projections from somatosensory and motor areas**

665 To establish a 3D benchmark map of corticopontine projections from somatosensory and
666 motor areas in in adult wild type mice, we utilized a selection of public experimental tract-
667 tracing data available from the Allen Institute mouse brain connectivity atlas
668 (http://connectivity.brain-map.org/). We selected 11 experiments in which the anterograde
669 tracer EGFP was injected in the right primary/secondary motor cortex (n =6) or primary
670 somatosensory cortex (n = 5) of wild type C57BL/6J mice (**Supplementary Table 1**). Serial two
671 photon fluorescence images were interactively inspected online using the Projection High
672 Resolution Image viewer of the Allen Institute, and from each case, 5 sagittal oriented images
673 of the right pontine nuclei (matching the orientation of the histological material generated
674 from our knock-out mice), spaced at ~100 μm were captured by screen shot from the largest
675 3D multiplane thumbnail viewer. The resolution of the captured images was up-sampled
676 three times original size before their spatial alignment to the CCFv3 was optimized using the
677 tools QuickNII (Puchades et al., 2019) and VisuAlign (RRID), as described below. These images
678 were used to create 3D representations of the axonal labeling in the pontine nuclei (**Figure 2**;
679 see below).

680 **Animals**

681 All mice used were bred in a C57BL/6J background. Male and female animals at any stage of
682 development were used. All experiments were conducted in accordance with the French
683 Animal Welfare Act and European guidelines for the use of experimental animals, using
684 protocols approved by the French Ministry of Education, Research and Innovation and the
685 local ethics committee (CIEPAL NCE/2019–548, Nice) under authorization #15 349 and #15
686 350. *Nr2f1/COUP-TFI*$^{fl/fl}$ mice were crossed with *Emx1-Cre-recombinase* mice to inactivate
687 *Nr2f1/COUP-TFI* exclusively in cortical progenitors and their progeny (Armentano et al.,
688 2007b) or with *Nex-Cre-recombinase* mice to abolish *Nr2f1/COUP-TFI* expression from
689 postmitotic neurons (Alfano et al., 2014b). Littermate *Nr2f1/COUP-TFI*$^{fl/fl}$ mice without the
690 presence of the *Cre-recombinase* gene (*Cre-negatives*) were considered controls
691 (**Supplementary Table 2**). For postnatal (P)21 and adult topographic map analysis, *Emx1-cKO*

692 and *Nex-cKO* animals were further crossed with *Thy1-eYFP-H* mice to specifically label layer V
693 projection neurons, as previously reported (Harb et al., 2016; Porrero et al., 2010). Mice were
694 genotyped as previously described (Alfano et al., 2014b; Armentano et al., 2007b; Harb et al.,
695 2016). Control and mutant littermates were genotyped as *Nr2f1*$^{fl/fl}$*:Thy1-eYFP-H*$^{T/+}$ and
696 *Nr2f1*$^{fl/fl}$*:Emx1-Cre:Thy1-eYFP-H*$^{T/+}$ or *Nr2f1*$^{fl/fl}$*:Nex-Cre:Thy1-eYFP-H*$^{T/+}$, respectively. For
697 simplicity, mutant mice are named *Emx1-cKO* and *Nex-cKO* throughout the text. Midday of
698 the day of the observed vaginal plug was considered as embryonic day 0.5 (E0.5).

699 **Anterograde tracing of corticospinal axons in early postnatal mice**

700 P4-P5 animals were anesthetized on ice for 5 min and kept on ice during the whole procedure.
701 Viral particles were produced from the AAV9-CAGtdTomato plasmid by the Alexis Bemelmans
702 (CEA, France) Company, and diluted 1:50 in TE-Buffer (Qiagen, #1018499) to a final
703 concentration of 1.75e12 vg/ml (kindly donated by I. Dusart, Pierre and Marie Curie
704 University, Paris, France). Approximately 0.5/1ul was injected unilaterally in different rostral-
705 caudal and medio-lateral brain locations of control and *Nex-cKO* pups, as previously described
706 in (Gu et al. 2017).

707 **Microscopic imaging**

708 Mosaic microscopic images were acquired using an Axio Imager M2 epifluorescence
709 microscope (Carl Zeiss Microscopy GmbH, Jena, Germany) equipped with a halogen lamp, a
710 MCU 2008 motorized stage, and an EC Plan-Neofluar 10x/0.30 and an AxioCam MRm camera.
711 ZEN blue software was used for imaging and automatic stitching. Images were exported in
712 TIFF format and serially ordered from lateral to medial, rotated and if needed, mirrored to
713 consistent anatomical orientation using Adobe Photoshop CS6 (RRID: SCR_014199), before
714 being converted to PNG format and resized to 60% of original size using ImageJ
715 (RRID:SCR_003070) with bilinear interpolation. The resized serial images were loaded into
716 Adobe Photoshop as a stack, spatially aligned using the ventral surfaces of the pons and
717 cerebral peduncle as landmarks, cropped and exported as individual PNG files.

718 For comparative analyses of topographical organization (see below), variations in YFP signal
719 expression intensity within and between groups were normalized by adjusting the brightness

720 and contrast of images to equal levels using a custom-made histogram matching script
721 available for ImageJ (National Institutes of Health; https://imagej.nih.gov/). One selected,
722 representative case (Experiment 5, Cre-negative, nr: 14250, **Supplementary Table 2**) was
723 used as reference.

724 **Spatial alignment to common 3D reference atlas**

725 Serial sectional images were spatially registered to the *Allen Mouse Common Coordinate*
726 *Framework*, version 3, 2017 edition of the delineations (CCFv3, (Wang et al., 2020) using the
727 QuickNII software tool (RRID:SCR_016854; (Puchades et al., 2019). Multiple anatomical
728 landmarks (hippocampus, caudoputamen, inferior and superior colliculus, and external
729 surface of the neocortex) were used to determine the mediolateral position and orientation
730 of the sagittal section images. For each section image, custom atlas diagrams were aligned to
731 anatomical landmarks in the experimental images using affine transformations, with
732 emphasis on matching the ventral surface of the pons and white matter tracts close to the
733 pontine nuclei and exported as PNG images. As a secondary step, to further optimize
734 registration, the custom atlas images were non-linearly transformed using the software tool
735 VisuAlign v0.8 (RRID:SCR_017978), with particular focus on fitting the template to the outer
736 brain surface, subcortical white matter, and the outer boundaries of the pontine nuclei. To
737 co-display images and the spatially registered custom atlas images, we used the software tool
738 LocaliZoom, which is embedded in the Navigator3 image management system
739 (bit.ly/navigator3), developed and hosted by the Neural Systems Laboratory at the University
740 of Oslo, Norway.

741 **Cortical distribution analysis in *Emx1-cKO* and *Nex-cKO* mutants**

742 Serial section images from *Nex-cKO* and *Emx1-cKO* mutants co-registered to the *Allen Mouse*
743 *Brain Connectivity Atlas* were analyzed using an ImageJ macro allowing automatic counting
744 of spots by area of interest in the brain. The spots are considered as specific staining using a
745 threshold based on intensity and shape of the elements and the composite RGB segmentation
746 atlas as a mask for the region of interest. The macro will create 3 separate folders, one will
747 contain the atlas masks, a second will contain the raw TIFF data and finally a third folder that

748 will collect all the output images and excel files. MORE DETAILS ARE ILLUSTRATED AS AN
749 ANNEX IN THE RESPONSE OF THE REVIEWERS' DOCUMENT.

750 **Corticospinal tract morphometric analysis in *Emx1-cKO* and *Nex-cKO* mutants**

751 Serial section images from *Nex-cKO* and *Emx1-cKO* mutants were analyzed by using the *Fiji-*
752 *ImageJ Software* tool (Schindelin et al., 2015) used to determine the total dorsoventral width
753 of the bundle expressing fluorescent signal in the descending fiber tract in different positions:
754 rostrally and caudally to the pontine nuclei, and 250 µm and 500 µm caudal to the nuclei. The
755 width of separate fiber fascicles was also measured 250 µm and 500µm from the terminal
756 edge of the pontine nuclei (**Figure 4A'**).

757 **Analysis of tracer injection sites**

758 Serial section images of cortical tracer injections in *Nex-cKO* brains (**Supplementary Table 3**)
759 and experiments taken from the *Allen Mouse Brain Connectivity Atlas*, were spatially aligned
760 using QuickNII and VisuAlign, as described above. The center positions of the injection sites
761 were annotated as a point-coordinate using LocaliZoom, co-displayed with the CCFv3 atlas in
762 the 3D viewer tool MeshView (RRID:SCR_017222). These visualizations were used to select
763 spatially corresponding injection site locations for analyses of spatial distribution of
764 corticopontine projections.

765 **Histology, immunohistochemistry and *in situ* hybridization**

766 At P21 and adulthood, animals were anesthetized by intraperitoneal injection of a mixture of
767 Tiletamine-Zolazepam-Xylazine-Buprenorphine and intracardially perfused with PB Saline
768 (PBS) followed by 4% paraformaldehyde (PFA) in PBS. Volumes were 15, 20 and 30 ml,
769 respectively. Brains were removed from the skull and postfixed for 4 h at 4°C in 4% PFA, before
770 being vibratome-sectioned in 100µm (adult samples) or 150µm (P21 samples) thick sagittal
771 sections. All sections were incubated overnight at 4°C in a solution of 0.5% Triton X-100, 3%
772 BSA, 10% goat serum in PBS, for permeabilization and reduction of non-specific binding of
773 antibodies. For immunofluorescence (IF), sections were incubated for 2 days at 4°C with
774 primary antibodies in a solution of 0.5% Triton X-100, 10% goat serum in PBS, and then
775 overnight at 4°C with relative secondary antibodies and HOECHST diluted in PBS. For the

complete list of primary and secondary antibodies, see **Supplementary Table 5**. Sections were washed several times in PBS, then transferred on Superfrost plus slides (ThermoScientific), covered and dried for 30 min to 1 h, and finally mounted with the Mowiol (Sigma-Aldrich) mounting medium.

Semi-quantitative recording and 3D visualization of spatial distribution patterns

To investigate and compare the 3D distributions of YFP signal expression or anterograde axonal labelling within the pontine nuclei, we used the annotation functionality in the LocaliZoom tool to semi-quantitatively record YFP signal expression or labelled axons in all sections through the pontine nuclei as point coordinates (specified in the coordinate system of the reference atlas, CCFv3), reflecting the overall density of signal/labelling observed in the images (**Figure 2C-D)**. To compensate for the spacing between sections and allow inspection of point distributions perpendicularly to the section angle, the z-coordinate of each point was randomly displaced within the thickness of the gap between sections using a custom Python script. The point-coordinates were co-displayed in the MeshView 3D viewer tool (**Figures 2, 5, 6, 7)**.

Data and Code Availability

All microscopic images and derived 3D point coordinate data representing the YFP signal expression or axonal labelling in the pontine nuclei generated in this project will be shared via the EBRAINS research infrastructure (https://search.kg.ebrains.eu/) as high-resolution TIFF images, together with customized, spatially matching reference atlas plates in PNG format. The custom Python script (spread.py) used to randomly displace data points within the thickness of a section is available upon request. The LocaliZoom and Meshview viewer tools are available from https://search.kg.ebrains.eu/

SUPPLEMENTARY FIGURES

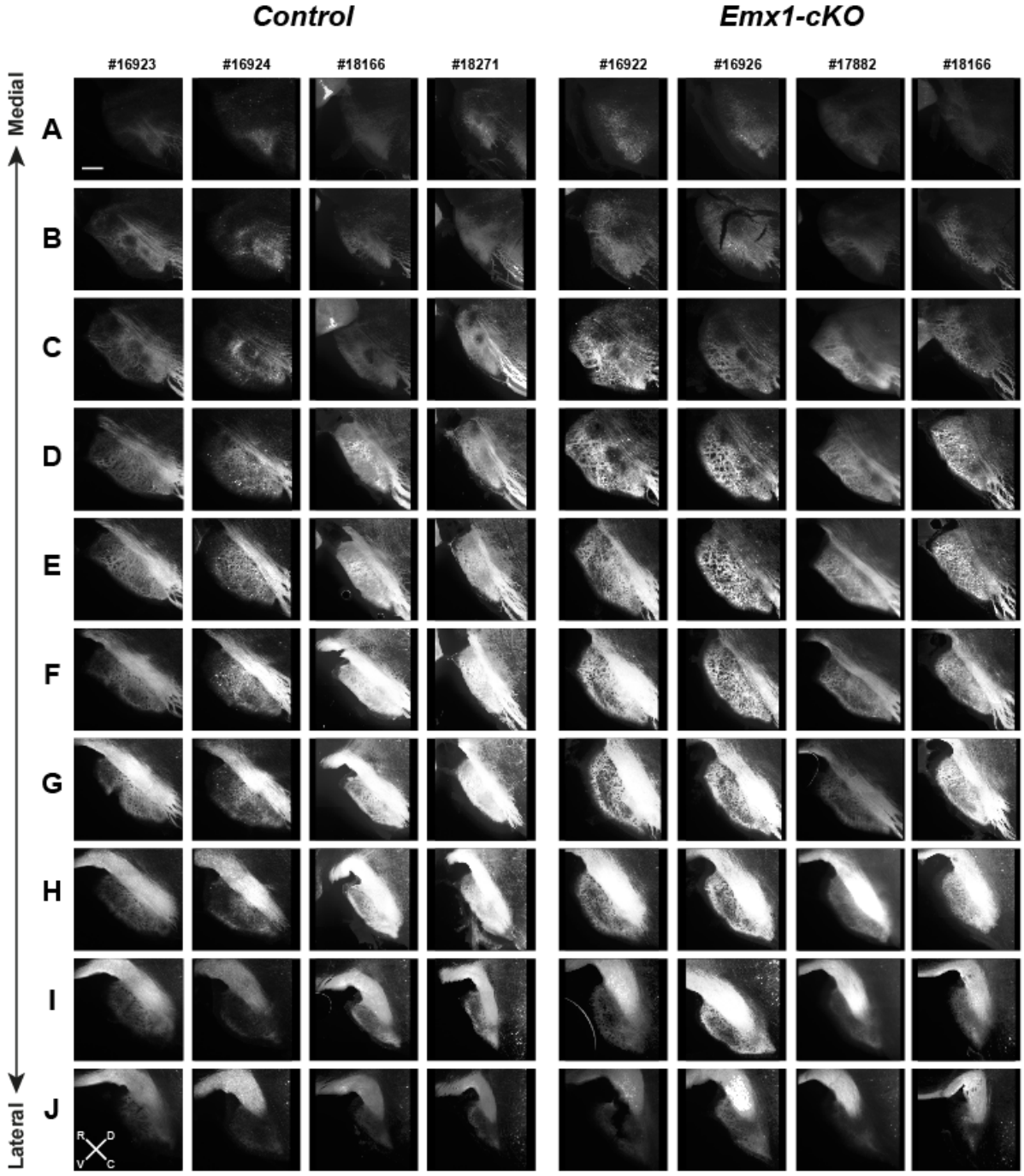

Supplementary Figure 1. *Fluorescence microscopy images of the pontine nuclei in sagittal sections from 4 control- and 4 Emx1-cKO mice. Columns show images from one animal, with sections from corresponding levels from medial to lateral are sorted from top to bottom (rows A-J). The intensity levels of the images have been normalized. Signal expression in Emx1-cKO mice is more widespread and more diffusely distributed in the pontine nuclei, relative to controls. Scale bar, 200 µm.*

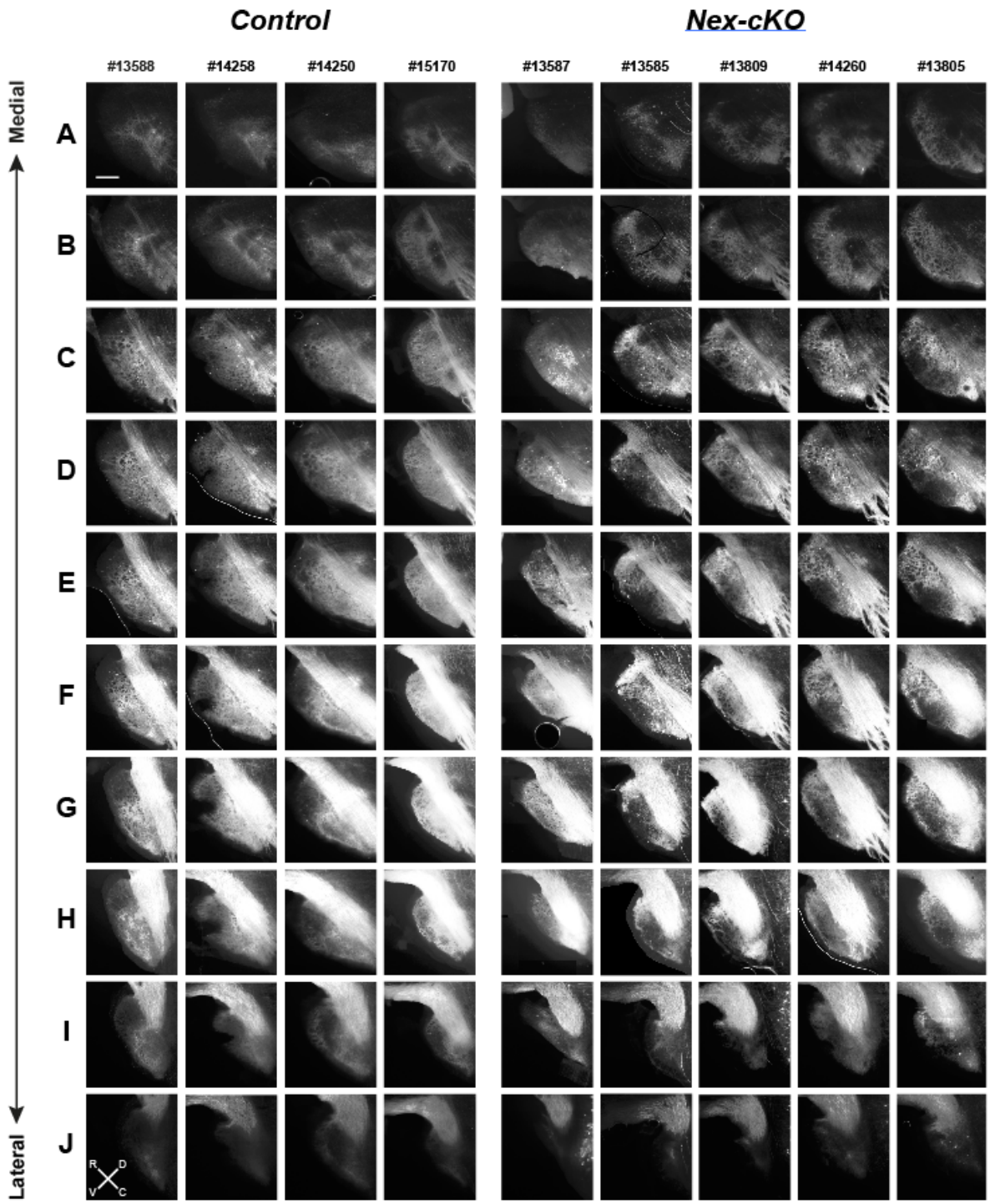

Supplementary Figure 2. *Fluorescence microscopy images of the pontine nuclei in sagittal sections from 4 control- and 4 Nex-cKO mice. Columns show images from one animal, with sections from corresponding levels from medial to lateral are sorted from top to bottom (rows A-J). The intensity levels of the images have been normalized. Signal expression in Nex-cKO mice is more clearly reduced or absent in the central core region of the pontine nuclei, relative to controls. Scale bar, 200 µm.*

IN THE FINAL VERSION, WE WILL ADD A NEW **SUPPLEMENTARY FIGURE 3** SHOWING THE PONTINE NUCLEI OF ALL SPECIMEN INJECTED WITH THE AAV9-CAGtdTomato VIRUS AND ANALYSED IN THIS STUDY.

819 **SUPPLEMENTARY TABLES**

820 ***Supplementary Table 1***

Allen Mouse Brain Connectivity database					
Experiment number #	**Sex**	**Age (±2)**	**Genotype**	**Injection site**	**Shown in**
100141780	Male	P56	C57BL/6J	Primary motor cortex	Fig. 2, 6A-F
114290938	male	P56	C57BL/6J	Primary somatosensory cortex, mouth region	Fig. 2A-P, 7A and 7H
112229814	male	P56	C57BL/6J	Primary somatosensory cortex, upper limb region	Fig. 2, 7B and 7F
112952510	male	P56	C57BL/6J	Secondary motor cortex	Fig. 2
114292355	male	P56	C57BL/6J	Primary somatosensory cortex, lower limb region	Fig. 2, 7A and 7D
126908007	male	P56	C57BL/6J	Primary somatosensory cortex, nose region	Fig. 2, 7A and 7G
127084296	male	P56	C57BL/6J	Secondary motor cortex	Fig. 2
127866392	male	P56	C57BL/6J	Primary somatosensory cortex, barrel field region	Fig. 2
141602484	male	P56	C57BL/6J	Secondary motor cortex	Fig. 2
141603190	male	P56	C57BL/6J	Secondary motor cortex	Fig. 2
585025284	male	P56	C57BL/6J	Secondary motor cortex	Fig. 2

821

822 ***Supplementary Table 2***

Adult					
Exp. #	**Animal #**	**Sex**	**Age**	**Genotype**	**Shown in**
1	13588	female	P33	*Thy1-eYFP$^{T/+}$; Nr2f1$^{fl/fl}$*	Fig. 3, 4, 5 and Suppl. Fig.1, 2
1	13587	female	P33	*Thy1-eYFP$^{T/+}$; Nr2f1$^{/fl}$; Nex-Cre*	Fig. 3, 4, 5 and Suppl. Fig.1, 2
2	13585	male	P62	*Thy1-eYFP$^{T/+}$; Nr2f1$^{/fl}$; Nex-Cre*	Fig. 3, 4, 5 and Suppl. Fig.1, 2
3	13809	male	P57	*Thy1-eYFP$^{T/+}$; Nr2f1$^{/fl}$; Nex-Cre*	Fig. 3, 4, 5 and Suppl. Fig.1, 2
4	14258	male	P57	*Thy1-eYFP$^{T/+}$; Nr2f1$^{/fl}$*	Fig. 3, 4, 5 and Suppl. Fig.1, 2
4	14260	male	P57	*Thy1-eYFP$^{T/+}$; Nr2f1$^{/fl}$; Nex-Cre*	Fig. 3, 4, 5 and Suppl. Fig.1, 2
5	13805	male	P55	*Thy1-eYFP$^{T/+}$; Nr2f1$^{/fl}$; Nex-Cre*	Fig. 3, 4, 5 and Suppl. Fig.1, 2
5	14250	male	P72	*Thy1-eYFP$^{T/+}$; Nr2f1$^{/fl}$*	Fig. 3, 4, 5 and Suppl. Fig.1, 2
5	15170	male	P75	*Thy1-eYFP$^{T/+}$; Nr2f1$^{/fl}$*	Fig. 3, 4, 5 and Suppl. Fig.1, 2
6	16922	male	P76	*Thy1-eYFP$^{T/+}$; Nr2f1$^{/fl}$; Emx1-Cre*	Fig. 3, 4, 5 and Suppl. Fig.1, 2
6	16923	male	P76	*Thy1-eYFP$^{T/+}$; Nr2f1$^{/fl}$*	Fig. 3, 4, 5 and Suppl. Fig.1, 2
6	16924	male	P76	*Thy1-eYFP$^{T/+}$; Nr2f1$^{/fl}$*	Fig. 3, 4, 5 and Suppl. Fig.1, 2
6	16926	male	P76	*Thy1-eYFP$^{T/+}$; Nr2f1$^{/fl}$; Emx1-Cre*	Fig. 3, 4, 5 and Suppl. Fig.1, 2
7	17882	male	P72	*Thy1-eYFP$^{T/+}$; Nr2f1$^{/fl}$; Emx1-Cre*	Fig. 3, 4, 5 and Suppl. Fig.1, 2
8	18046	female	P109	*Thy1-eYFP$^{T/+}$; Nr2f1$^{/fl}$; Emx1-Cre*	Fig. 3, 4, 5 and Suppl. Fig.1, 2
8	18166	female	P98	*Thy1-eYFP$^{T/+}$; Nr2f1$^{/fl}$*	Fig. 3, 4, 5 and Suppl. Fig.1, 2
8	18271	female	P87	*Thy1-eYFP$^{T/+}$; Nr2f1$^{/fl}$*	Fig. 3, 4, 5 and Suppl. Fig.1, 2
9	19606	female	P86	*Thy1-eYFP$^{T/+}$; Nr2f1$^{/fl}$; Emx1-Cre*	Fig. 4
9	19607	female	P86	*Thy1-eYFP$^{T/+}$; Nr2f1$^{/fl}$; Emx1-Cre*	Fig. 4

823

824 ***Supplementary Table 3***

P21 – unilateral CST tracing			
Tracer injected in motor cortex			
Experiment #	**Animal #**	**Genotype**	**Shown in**
2	11643_13	*Ctrl*	Fig. 6A and 7B
2	11643_16	*Nex-cKO*	Suppl. Fig. 3
2	11643_17	*Nex-cKO*	Fig. 6A and 6F
2	11796_2	*Ctrl*	Suppl. Fig. 3
2	11796_8	*Ctrl*	Suppl. Fig. 3
2	11796_9	*Ctrl*	Suppl. Fig. 3
3	18035_1	*Ctrl*	Fig. 6A and 6F
3	18035_2	*Ctrl*	Fig. 6A and 6E
3	18035_7	*Ctrl*	Suppl. Fig. 3
3	18035_3	*Nex-cKO*	Fig. 6A and 6E
3	18035_4	*Nex-cKO*	Suppl. Fig. 3
3	18035_8	*Nex-cKO*	Fig. 6A and 76D
4	19423_2	*Ctrl*	Suppl. Fig. 3
4	19423_3	*Ctrl*	Suppl. Fig. 3
4	19423_4	*Nex-cKO*	Suppl. Fig. 3
4	19423_5	*Nex-cKO*	Suppl. Fig. 3
Tracer injected in somatosensory cortex			
4	19423_6	*Nex-cKO*	Fig. 7A and 7D
4	19423_7	*Nex-cKO*	Fig. 7A and 7E
6	11431_1	*Nex-cKO*	Fig. 7A and 7G
6	11431_3	*Nex-cKO*	Fig. 7A and 7H
6	11431_4	*Nex-cKO*	Fig. 7A and 7F
6	11431_6	*Ctrl*	Fig. 7A and 7F
6	11431_7	*Nex-cKO*	Fig. 7A and 7H

825
826
827

828 ***Supplementary Table 4:***

829

Figure 3 – Cortical distribution of YFP-H positive cells							
Area	**Hypothesis**	**Mean 1**	**Mean 2**	**Mean diff.**	**95,00% CI of diff**	**Summary**	**Adjusted P.**
PFC	*Ctrl vs. Nex-cKO*	1.172	0.3174	0.8543	-0.209 to 1.918	ns	0.3142
	Ctrl vs. Emx1-cKO	1.172	0.9523	0.2194	-0.8439 to 1.283	ns	>0.9999
	Nex-cKO vs. Emx1-cKO	0.3174	0.9523	-0.6349	-1.8 to 0.5299	ns	>0.9999
ACC	*Ctrl vs. Nex-cKO*	2.411	1.104	1.307	0.2434 to 2.37	**	0.0042
	Ctrl vs. Emx1-cKO	2.411	1.411	1	-0.06316 to 2.063	ns	0.0897
	Nex-cKO vs. Emx1-cKO	1.104	1.411	-0.3065	-1.471 to 0.8583	ns	>0.9999
GC	*Ctrl vs. Nex-cKO*	0.5317	0.09524	0.4365	-0.7283 to 1.601	****	<0.0001
	Ctrl vs. Emx1-cKO	0.5317	0.09524	0.4365	-0.7283 to 1.601	ns	0.1008
	Nex-cKO vs. Emx1-cKO	0.09524	0.09524	0	-1.345 to 1.345	***	0.0001
M2	*Ctrl vs. Nex-cKO*	1.515	2.773	1.515	1.709 to 3.836	****	<0.0001
	Ctrl vs. Emx1-cKO	3.301	0.9872	3.301	-0.07613 to 2.051	ns	>0.9999
	Nex-cKO vs. Emx1-cKO	3.301	-1.785	3.301	-2.95 to -0.6207	****	<0.0001
M1	*Ctrl vs. Nex-cKO*	4.217	1.818	2.399	1.336 to 3.462	ns	>0.9999
	Ctrl vs. Emx1-cKO	4.217	3.703	0.5139	-0.5495 to 1.577	**	0.0016
	Nex-cKO vs. Emx1-cKO	1.818	3.703	-1.885	-3.05 to -0.7202	****	<0.0001
S1	*Ctrl vs. Nex-cKO*	3.346	2.922	0.4237	-0.6396 to 1.487	ns	>0.9999
	Ctrl vs. Emx1-cKO	3.346	4.74	-1.394	-2.458 to -0.331	**	0.0016
	Nex-cKO vs. Emx1-cKO	2.922	4.74	-1.818	-2.983 to -0.6533	****	<0.0001
A	*Ctrl vs. Nex-cKO*	0.8868	1.803	-0.9158	-1.979 to 0.1475	ns	0.1883
	Ctrl vs. Emx1-cKO	0.8868	3.66	-2.773	-3.836 to -1.71	****	<0.0001
	Nex-cKO vs. Emx1-cKO	1.803	3.66	-1.857	-3.022 to -0.6922	****	<0.0001
V	*Ctrl vs. Nex-cKO*	0.9544	2.686	-1.732	-2.795 to -0.6684	****	<0.0001
	Ctrl vs. Emx1-cKO	0.9544	4.045	-3.091	-4.154 to -2.027	****	<0.0001
	Nex-cKO vs. Emx1-cKO	2.686	4.045	-1.359	-2.524 to -0.1942	**	0.0086
RSC	*Ctrl vs. Nex-cKO*	0.8826	2.101	-1.219	-2.282 to -0.1553	*	0.0108
	Ctrl vs. Emx1-cKO	0.8826	3.024	-2.142	-3.205 to -1.078	****	<0.0001
	Nex-cKO vs. Emx1-cKO	2.101	3.024	-0.923	-2.088 to 0.2418	ns	0.3454
Figure 4E – Rostral LFP diameter							
Section	**Hypothesis**	**Mean 1**	**Mean 2**	**Mean diff.**	**95,00% CI of diff**	**Summary**	**Adjusted P.**
1	*Ctrl vs. Nex-cKO*	0	0	0	-116.9 to 116.9	ns	>0.9999
	Ctrl vs. Emx1-cKO	0	0	0	-116.9 to 116.9	ns	>0.9999
	Nex-cKO vs. Emx1-cKO	0	0	0	-124.9 to 124.9	ns	>0.9999
2	*Ctrl vs. Nex-cKO*	0	28.29	-28.29	-145.2 to 88.57	ns	0.836
	Ctrl vs. Emx1-cKO	0	0	0	-116.9 to 116.9	ns	>0.9999
	Nex-cKO vs. Emx1-cKO	28.29	0	28.29	-96.64 to 153.2	ns	0.8549
3	*Ctrl vs. Nex-cKO*	0	132.7	-132.7	-249.6 to -15.84	*	0.0215
	Ctrl vs. Emx1-cKO	0	0	0	-116.9 to 116.9	ns	>0.9999
	Nex-cKO vs. Emx1-cKO	132.7	0	132.7	7.775 to 257.6	*	0.0343
4	*Ctrl vs. Nex-cKO*	0	179.6	-179.6	-296.5 to -62.77	**	0.001
	Ctrl vs. Emx1-cKO	0	0	0	-116.9 to 116.9	ns	>0.9999
	Nex-cKO vs. Emx1-cKO	179.6	0	179.6	54.71 to 304.6	**	0.0023
5	*Ctrl vs. Nex-cKO*	0	175.9	-175.9	-292.8 to -59.04	**	0.0013
	Ctrl vs. Emx1-cKO	0	55.34	-55.34	-172.2 to 61.52	ns	0.5052
	Nex-cKO vs. Emx1-cKO	175.9	55.34	120.6	-4.369 to 245.5	ns	0.0612
6	*Ctrl vs. Nex-cKO*	24.35	169.6	-145.2	-262.1 to -28.37	*	0.0103
	Ctrl vs. Emx1-cKO	24.35	115	-90.67	-207.5 to 26.2	ns	0.1624
	Nex-cKO vs. Emx1-cKO	169.6	115	54.57	-70.37 to 179.5	ns	0.5592
7	*Ctrl vs. Nex-cKO*	117	231.4	-114.4	-231.3 to 2.467	ns	0.0565
	Ctrl vs. Emx1-cKO	117	234.6	-117.7	-234.5 to -0.8201	*	0.048
	Nex-cKO vs. Emx1-cKO	231.4	234.6	-3.287	-128.2 to 121.6	ns	0.9979
8	*Ctrl vs. Nex-cKO*	241.7	187.5	54.13	-66.26 to 174.5	ns	0.5401
	Ctrl vs. Emx1-cKO	241.7	293	-51.33	-171.7 to 69.06	ns	0.5746
	Nex-cKO vs. Emx1-cKO	187.5	293	-105.5	-230.4 to 19.47	ns	0.1168
9	*Ctrl vs. Nex-cKO*	316.6	267.9	48.71	-68.15 to 165.6	ns	0.5888
	Ctrl vs. Emx1-cKO	316.6	250.1	66.55	-56.81 to 189.9	ns	0.4128
	Nex-cKO vs. Emx1-cKO	267.9	250.1	17.83	-113.2 to 148.9	ns	0.9449
10	*Ctrl vs. Nex-cKO*	318.9	194.4	124.6	7.715 to 241.4	*	0.0335
	Ctrl vs. Emx1-cKO	318.9	205.8	113.1	-3.738 to 230	ns	0.0602
	Nex-cKO vs. Emx1-cKO	194.4	205.8	-11.45	-136.4 to 113.5	ns	0.9746
11	*Ctrl vs. Nex-cKO*	231.1	88.06	143.1	-163 to 449.1	ns	0.514
	Ctrl vs. Emx1-cKO	231.1	64.04	167.1	-82.79 to 416.9	ns	0.258
	Nex-cKO vs. Emx1-cKO	88.06	64.04	24.02	-225.8 to 273.9	ns	0.9721

12	*Ctrl vs. Nex-cKO*	276.1	179.6	96.5	-26.86 to 219.9	ns	0.1576
	Ctrl vs. Emx1-cKO	276.1	136.5	139.6	16.23 to 263	*	0.022
	Nex-cKO vs. Emx1-cKO	179.6	136.5	43.09	-93.77 to 179.9	ns	0.7389
13	*Ctrl vs. Nex-cKO*	201.9	180.5	21.33	-243.7 to 286.3	ns	0.9804
	Ctrl vs. Emx1-cKO	201.9	44.45	157.4	-40.14 to 354.9	ns	0.1471
	Nex-cKO vs. Emx1-cKO	180.5	44.45	136.1	-113.8 to 385.9	ns	0.4059
14	*Ctrl vs. Nex-cKO*	218.4	114.6	103.8	-19.52 to 227.2	ns	0.1182
	Ctrl vs. Emx1-cKO	218.4	95.41	123	-0.3344 to 246.4	ns	0.0508
	Nex-cKO vs. Emx1-cKO	114.6	95.41	19.19	-117.7 to 156	ns	0.9416
15	*Ctrl vs. Nex-cKO*	154.7	59.11	95.61	-21.25 to 212.5	ns	0.1328
	Ctrl vs. Emx1-cKO	154.7	51.17	103.6	-13.31 to 220.4	ns	0.0942
	Nex-cKO vs. Emx1-cKO	59.11	51.17	7.94	-117 to 132.9	ns	0.9877
16	*Ctrl vs. Nex-cKO*	101.6	16.85	84.78	-32.09 to 201.6	ns	0.2035
	Ctrl vs. Emx1-cKO	101.6	18.75	82.87	-33.99 to 199.7	ns	0.2183
	Nex-cKO vs. Emx1-cKO	16.85	18.75	-1.908	-126.8 to 123	ns	0.9993
17	*Ctrl vs. Nex-cKO*	60.94	0	60.94	-55.93 to 177.8	ns	0.4374
	Ctrl vs. Emx1-cKO	60.94	0	60.94	-55.93 to 177.8	ns	0.4374
	Nex-cKO vs. Emx1-cKO	0	0	0	-124.9 to 124.9	ns	>0.9999
18	*Ctrl vs. Nex-cKO*	28.85	0	28.85	-88.02 to 145.7	ns	0.8301
	Ctrl vs. Emx1-cKO	28.85	0	28.85	-88.02 to 145.7	ns	0.8301
	Nex-cKO vs. Emx1-cKO	0	0	0	-124.9 to 124.9	ns	>0.9999
19	*Ctrl vs. Nex-cKO*	0	0	0	-112 to 112	ns	>0.9999
	Ctrl vs. Emx1-cKO	0	0	0	-116.9 to 116.9	ns	>0.9999
	Nex-cKO vs. Emx1-cKO	0	0	0	-120.4 to 120.4	ns	>0.9999

Figure 4F – Caudal LFP diameter

Section	Hypothesis	Mean 1	Mean 2	Mean diff.	95,00% CI of diff	Summary	Adjusted P.
1	*Ctrl vs. Nex-cKO*	0	0	0	-88.51 to 88.51	ns	>0.9999
	Ctrl vs. Emx1-cKO	0	0	0	-88.51 to 88.51	ns	>0.9999
	Nex-cKO vs. Emx1-cKO	0	0	0	-94.62 to 94.62	ns	>0.9999
2	*Ctrl vs. Nex-cKO*	0	46.89	-46.89	-135.4 to 41.62	ns	0.4252
	Ctrl vs. Emx1-cKO	0	0	0	-88.51 to 88.51	ns	>0.9999
	Nex-cKO vs. Emx1-cKO	46.89	0	46.89	-47.73 to 141.5	ns	0.4728
3	*Ctrl vs. Nex-cKO*	0	98.1	-98.1	-186.6 to -9.584	*	0.0257
	Ctrl vs. Emx1-cKO	0	0	0	-88.51 to 88.51	ns	>0.9999
	Nex-cKO vs. Emx1-cKO	98.1	0	98.1	3.473 to 192.7	*	0.0402
4	*Ctrl vs. Nex-cKO*	0	126.2	-126.2	-214.7 to -37.72	**	0.0026
	Ctrl vs. Emx1-cKO	0	0	0	-88.51 to 88.51	ns	>0.9999
	Nex-cKO vs. Emx1-cKO	126.2	0	126.2	31.6 to 220.9	**	0.0053
5	*Ctrl vs. Nex-cKO*	18.5	111	-92.51	-181 to -3.999	*	0.0382
	Ctrl vs. Emx1-cKO	18.5	13.31	5.196	-83.32 to 93.71	ns	0.9895
	Nex-cKO vs. Emx1-cKO	111	13.31	97.71	3.084 to 192.3	*	0.0412
6	*Ctrl vs. Nex-cKO*	69.28	128.1	-58.82	-147.3 to 29.69	ns	0.2617
	Ctrl vs. Emx1-cKO	69.28	97.47	-28.19	-116.7 to 60.32	ns	0.7331
	Nex-cKO vs. Emx1-cKO	128.1	97.47	30.63	-63.99 to 125.3	ns	0.7256
7	*Ctrl vs. Nex-cKO*	107.5	176	-68.56	-300.3 to 163.2	ns	0.765
	Ctrl vs. Emx1-cKO	107.5	152.1	-44.66	-227.9 to 138.6	ns	0.8336
	Nex-cKO vs. Emx1-cKO	176	152.1	23.9	-159.3 to 207.1	ns	0.9491
8	*Ctrl vs. Nex-cKO*	175.2	237.2	-61.95	-157.9 to 34.02	ns	0.2821
	Ctrl vs. Emx1-cKO	175.2	154.5	20.69	-70.49 to 111.9	ns	0.8541
	Nex-cKO vs. Emx1-cKO	237.2	154.5	82.63	-16.61 to 181.9	ns	0.1235
9	*Ctrl vs. Nex-cKO*	214.5	138.2	76.34	-12.17 to 164.9	ns	0.1063
	Ctrl vs. Emx1-cKO	214.5	197.7	16.82	-71.69 to 105.3	ns	0.8952
	Nex-cKO vs. Emx1-cKO	138.2	197.7	-59.52	-154.1 to 35.1	ns	0.3005
10	*Ctrl vs. Nex-cKO*	209.6	115.1	94.49	5.983 to 183	*	0.0333
	Ctrl vs. Emx1-cKO	209.6	132	77.6	-10.91 to 166.1	ns	0.0988
	Nex-cKO vs. Emx1-cKO	115.1	132	-16.89	-111.5 to 77.73	ns	0.9069
11	*Ctrl vs. Nex-cKO*	232.5	99.13	133.4	44.9 to 221.9	**	0.0013
	Ctrl vs. Emx1-cKO	232.5	116.2	116.4	27.87 to 204.9	**	0.0061
	Nex-cKO vs. Emx1-cKO	99.13	116.2	-17.03	-111.7 to 77.59	ns	0.9055
12	*Ctrl vs. Nex-cKO*	186.4	127.8	58.65	-34.78 to 152.1	ns	0.302
	Ctrl vs. Emx1-cKO	186.4	26.38	160.1	71.56 to 248.6	****	<0.0001
	Nex-cKO vs. Emx1-cKO	127.8	26.38	101.4	2.179 to 200.7	*	0.0439
13	*Ctrl vs. Nex-cKO*	94.47	0	94.47	-137.3 to 326.2	ns	0.6019
	Ctrl vs. Emx1-cKO	94.47	13.38	81.09	-95.93 to 258.1	ns	0.527
	Nex-cKO vs. Emx1-cKO	0	13.38	-13.38	-190.4 to 163.6	ns	0.9826

14	*Ctrl vs. Nex-cKO*	58.1	0	58.1	-33.08 to 149.3	ns	0.2913
	Ctrl vs. Emx1-cKO	58.1	0	58.1	-33.08 to 149.3	ns	0.2913
	Nex-cKO vs. Emx1-cKO	0	0	0	-94.62 to 94.62	ns	>0.9999
15	*Ctrl vs. Nex-cKO*	0	0	0	-84.82 to 84.82	ns	>0.9999
	Ctrl vs. Emx1-cKO	0	0	0	-88.51 to 88.51	ns	>0.9999
	Nex-cKO vs. Emx1-cKO	0	0	0	-91.18 to 91.18	ns	>0.9999
Figure 4G – Rostral LFP area							
	Hypothesis	**Mean 1**	**Mean 2**	**Mean diff.**	**95,00% CI of diff**	**Summary**	**Adjusted P.**
	Ctrl vs. Nex-cKO	2414	2258	156.4	-570.3 to 883	ns	0.8257
	Ctrl vs. Emx1-cKO	2414	1725	689.2	-37.42 to 1416	ns	0.0637
Figure 4H – Caudal LFP area							
	Hypothesis	**Mean 1**	**Mean 2**	**Mean diff.**	**95,00% CI of diff**	**Summary**	**Adjusted P.**
	Ctrl vs. Nex-cKO	1403	1427	-24.29	-261.8 to 213.2	ns	0.9566
	Ctrl vs. Emx1-cKO	1403	884.1	518.8	281.3 to 756.3	***	0.0001
Figure 4I – Fasciculation Index							
Region	**Hypothesis**	**Mean 1**	**Mean 2**	**Mean diff.**	**95,00% CI of diff**	**Summary**	**Adjusted P.**
250 μm	*Ctrl vs. Nex-cKO*	0.6528	0.5493	0.1035	0.01185 to 0.1951	*	0.0216
	Ctrl vs. Emx1-cKO	0.6528	0.5595	0.09326	0.001658 to 0.1849	*	0.0446
500 μm	*Ctrl vs. Nex-cKO*	0.674	0.5771	0.0969	0.00254 to 0.1913	*	0.0422
	Ctrl vs. Emx1-cKO	0.674	0.5146	0.1594	0.06502 to 0.2537	***	0.0004

Summary of statistical analysis and results. *Highlighted in blue, comparisons that produced statistically significant P-values. P-values are calculated by 2way ANOVA test (**Figures 4F and 5E-F**), or ordinary one-way ANOVA test (**Figures 5G-I**).*

Supplementary Table 5: List of primary and secondary antibodies used in this study.

Antigen	Provider	Catalog #	Species	Working dilution
GFP	Abcam	Ab13970	Ck	1:500
RFP	Abcam	Ab 124754	Rb	1:500
Ck IgY - AF 488	Thermo Fisher	A11039	Gt	1:500
Rb IgG - AF 555	Thermo Fisher	A21428	Gt	1:500

REFERENCES:Uncategorized References

Alfano, C., Magrinelli, E., Harb, K., Hevner, R. F. and Studer, M. (2014a). Postmitotic control of sensory area specification during neocortical development. *Nature communications* **5**, 5632.(2014b). Postmitotic control of sensory area specification during neocortical development. *Nature communications* **5**, 5632.

Alfano, C. and Studer, M. (2012). Neocortical arealization: Evolution, mechanisms and open questions. *Dev Neurobiol*.

Altman, J. and Bayer, S. A. (1987). Development of the precerebellar nuclei in the rat: IV. The anterior precerebellar extramural migratory stream and the nucleus reticularis tegmenti pontis and the basal pontine gray. *J Comp Neurol* **257**, 529-552.

Armentano, M., Chou, S. J., Tomassy, G. S., Leingartner, A., O'Leary, D. D. and Studer, M. (2007a). COUP-TFI regulates the balance of cortical patterning between frontal/motor and sensory areas. *Nature neuroscience* **10**, 1277-1286.

---- (2007b). COUP-TFI regulates the balance of cortical patterning between frontal/motor and sensory areas. *Nat Neurosci* **10**, 1277-1286.

Assimacopoulos, S., Kao, T., Issa, N. P. and Grove, E. A. (2012). Fibroblast growth factor 8 organizes the neocortical area map and regulates sensory map topography. *J Neurosci* **32**, 7191-7201.

Badura, A., Schonewille, M., Voges, K., Galliano, E., Renier, N., Gao, Z., Witter, L., Hoebeek, F. E., Chedotal, A. and De Zeeuw, C. I. (2013). Climbing fiber input shapes reciprocity of Purkinje cell firing. *Neuron* **78**, 700-713.

Bertacchi, M., Parisot, J. and Studer, M. (2019). The pleiotropic transcriptional regulator COUP-TFI plays multiple roles in neural development and disease. *Brain Res* **1705**, 75-94.

Bjaalie, J. G. and Brodal, P. (1989). Visual pathways to the cerebellum: segregation in the pontine nuclei of terminal fields from different visual cortical areas in the cat. *Neuroscience* **29**, 95-107.

---- (1997). Cat pontocerebellar network: numerical capacity and axonal collateral branching of neurones in the pontine nuclei projecting to individual parafloccular folia. *Neurosci Res* **27**, 199-210.

Bower, J. M. (2011). Functional implications of tactile projection patterns to the lateral hemispheres of the cerebellum of the albino rat: the legacy of Wally Welker. *Annals of the New York Academy of Sciences* **1225**, 130-141.

Bower, J. M., Beermann, D. H., Gibson, J. M., Shambes, G. M. and Welker, W. (1981). Principles of organization of a cerebro-cerebellar circuit. Micromapping the projections from cerebral (SI) to cerebellar (granule cell layer) tactile areas of rats. *Brain, behavior and evolution* **18**, 1-18.

Bower, J. M. and Kassel, J. (1990). Variability in tactile projection patterns to cerebellar folia crus IIA of the Norway rat. *J Comp Neurol* **302**, 768-778.

Brodal, P. (1978). The corticopontine projection in the rhesus monkey. Origin and principles of organization. *Brain* **101**, 251-283.

Brodal, P. and Bjaalie, J. G. (1992). Organization of the pontine nuclei. *Neurosci Res* **13**, 83-118.

Buckner, R. L. (2013). The cerebellum and cognitive function: 25 years of insight from anatomy and neuroimaging. *Neuron* **80**, 807-815.

Cadwell, C. R., Bhaduri, A., Mostajo-Radji, M. A., Keefe, M. G. and Nowakowski, T. J. (2019). Development and Arealization of the Cerebral Cortex. *Neuron* **103**, 980-1004.

Cederquist, G. Y., Azim, E., Shnider, S. J., Padmanabhan, H. and Macklis, J. D. (2013). Lmo4 establishes rostral motor cortex projection neuron subtype diversity. *J Neurosci* **33**, 6321-6332.

Chapin, J. K. and Lin, C. S. (1984). Mapping the body representation in the SI cortex of anesthetized and awake rats. *J Comp Neurol* **229**, 199-213.

D'Elia, K. P. and Dasen, J. S. (2018). Topographic Maps: Motor Axons Wait Their Turn. *Curr Biol* **28**, R86-R88.

892 **Del Pino, I., Tocco, C., Magrinelli, E., Marcantoni, A., Ferraguto, C., Tomagra, G.,**
893 **Bertacchi, M., Alfano, C., Leinekugel, X., Frick, A., et al.** (2020). COUP-TFI/Nr2f1
894 Orchestrates Intrinsic Neuronal Activity during Development of the Somatosensory
895 Cortex. *Cereb Cortex* **30**, 5667-5685.
896 **Erzurumlu, R. S., Murakami, Y. and Rijli, F. M.** (2010). Mapping the face in the
897 somatosensory brainstem. *Nat Rev Neurosci* **11**, 252-263.
898 **Fabri, M. and Burton, H.** (1991). Ipsilateral cortical connections of primary somatic sensory
899 cortex in rats. *J Comp Neurol* **311**, 405-424.
900 **Feng, G., Mellor, R. H., Bernstein, M., Keller-Peck, C., Nguyen, Q. T., Wallace, M.,**
901 **Nerbonne, J. M., Lichtman, J. W. and Sanes, J. R.** (2000). Imaging neuronal
902 subsets in transgenic mice expressing multiple spectral variants of GFP. *Neuron* **28**,
903 41-51.
904 **Flore, G., Di Ruberto, G., Parisot, J., Sannino, S., Russo, F., Illingworth, E. A., Studer,**
905 **M. and De Leonibus, E.** (2017). Gradient COUP-TFI Expression Is Required for
906 Functional Organization of the Hippocampal Septo-Temporal Longitudinal Axis.
907 *Cereb Cortex* **27**, 1629-1643.
908 **Fritzsch, B., Elliott, K. L. and Pavlinkova, G.** (2019). Primary sensory map formations
909 reflect unique needs and molecular cues specific to each sensory system. *F1000Res*
910 **8**.
911 **Goebbels, S., Bormuth, I., Bode, U., Hermanson, O., Schwab, M. H. and Nave, K. A.**
912 (2006). Genetic targeting of principal neurons in neocortex and hippocampus of NEX-
913 Cre mice. *Genesis* **44**, 611-621.
914 **Greig, L. C., Woodworth, M. B., Galazo, M. J., Padmanabhan, H. and Macklis, J. D.**
915 (2013). Molecular logic of neocortical projection neuron specification, development
916 and diversity. *Nat Rev Neurosci* **14**, 755-769.
917 **Harb, K., Magrinelli, E., Nicolas, C. S., Lukianets, N., Frangeul, L., Pietri, M., Sun, T.,**
918 **Sandoz, G., Grammont, F., Jabaudon, D., et al.** (2016). Area-specific development
919 of distinct projection neuron subclasses is regulated by postnatal epigenetic
920 modifications. *eLife* **5**.
921 **Heffner, C. D., Lumsden, A. G. and O'Leary, D. D.** (1990). Target control of collateral
922 extension and directional axon growth in the mammalian brain. *Science* **247**, 217-
923 220.
924 **Henschke, J. U. and Pakan, J. M.** (2020). Disynaptic cerebrocerebellar pathways
925 originating from multiple functionally distinct cortical areas. *eLife* **9**.
926 **Inoue, K., Terashima, T. and Inoue, Y.** (1991). Postnatal development of the pontine
927 projections from the visual cortex of the mouse. *Okajimas Folia Anat Jpn* **67**, 479-
928 492.
929 **Leergaard, T. B.** (2003). Clustered and laminar topographic patterns in rat cerebro-pontine
930 pathways. *Anat Embryol (Berl)* **206**, 149-162.
931 **Leergaard, T. B., Alloway, K. D., Mutic, J. J. and Bjaalie, J. G.** (2000a). Three-
932 dimensional topography of corticopontine projections from rat barrel cortex:
933 correlations with corticostriatal organization. *J Neurosci* **20**, 8474-8484.
934 **Leergaard, T. B., Alloway, K. D., Pham, T. A., Bolstad, I., Hoffer, Z. S., Pettersen, C. and**
935 **Bjaalie, J. G.** (2004). Three-dimensional topography of corticopontine projections
936 from rat sensorimotor cortex: comparisons with corticostriatal projections reveal
937 diverse integrative organization. *J Comp Neurol* **478**, 306-322.
938 **Leergaard, T. B. and Bjaalie, J. G.** (1995). Semi-automatic data acquisition for quantitative
939 neuroanatomy. MicroTrace--computer programme for recording of the spatial
940 distribution of neuronal populations. *Neurosci Res* **22**, 231-243.
941 **----** (2007). Topography of the complete corticopontine projection: from experiments to
942 principal Maps. *Front Neurosci* **1**, 211-223.
943 **Leergaard, T. B., Lakke, E. A. and Bjaalie, J. G.** (1995). Topographical organization in the
944 early postnatal corticopontine projection: a carbocyanine dye and 3-D computer
945 reconstruction study in the rat. *J Comp Neurol* **361**, 77-94.

Leergaard, T. B., Lillehaug, S., De Schutter, E., Bower, J. M. and Bjaalie, J. G. (2006). Topographical organization of pathways from somatosensory cortex through the pontine nuclei to tactile regions of the rat cerebellar hemispheres. *Eur J Neurosci* **24**, 2801-2812.

Leergaard, T. B., Lyngstad, K. A., Thompson, J. H., Taeymans, S., Vos, B. P., De Schutter, E., Bower, J. M. and Bjaalie, J. G. (2000b). Rat somatosensory cerebropontocerebellar pathways: spatial relationships of the somatotopic map of the primary somatosensory cortex are preserved in a three-dimensional clustered pontine map. *J Comp Neurol* **422**, 246-266.

Lemon, R. N. (2008). Descending pathways in motor control. *Annu Rev Neurosci* **31**, 195-218.

Lillehaug, S., Oyan, D., Leergaard, T. B. and Bjaalie, J. G. (2002). Comparison of semi-automatic and automatic data acquisition methods for studying three-dimensional distributions of large neuronal populations and axonal plexuses. *Network* **13**, 343-356.

Liu, Q., Dwyer, N. D. and O'Leary, D. D. (2000). Differential expression of COUP-TFI, CHL1, and two novel genes in developing neocortex identified by differential display PCR. *J Neurosci* **20**, 7682-7690.

Maheshwari, U., Kraus, D., Vilain, N., Holwerda, S. J. B., Cankovic, V., Maiorano, N. A., Kohler, H., Satoh, D., Sigrist, M., Arber, S., et al. (2020). Postmitotic Hoxa5 Expression Specifies Pontine Neuron Positional Identity and Input Connectivity of Cortical Afferent Subsets. *Cell reports* **31**, 107767.

McLaughlin, T. and O'Leary, D. D. (2005). Molecular gradients and development of retinotopic maps. *Annu Rev Neurosci* **28**, 327-355.

Mercurio, S., Serra, L., Motta, A., Gesuita, L., Sanchez-Arrones, L., Inverardi, F., Foglio, B., Barone, C., Kaimakis, P., Martynoga, B., et al. (2019). Sox2 Acts in Thalamic Neurons to Control the Development of Retina-Thalamus-Cortex Connectivity. *iScience* **15**, 257-273.

Mihailoff, G. A., Lee, H., Watt, C. B. and Yates, R. (1985). Projections to the basilar pontine nuclei from face sensory and motor regions of the cerebral cortex in the rat. *J Comp Neurol* **237**, 251-263.

Mottolese, C., Richard, N., Harquel, S., Szathmari, A., Sirigu, A. and Desmurget, M. (2013). Mapping motor representations in the human cerebellum. *Brain* **136**, 330-342.

Nitschke, M. F., Kleinschmidt, A., Wessel, K. and Frahm, J. (1996). Somatotopic motor representation in the human anterior cerebellum. A high-resolution functional MRI study. *Brain* **119 (Pt 3)**, 1023-1029.

O'Leary, D. D. and Nakagawa, Y. (2002). Patterning centers, regulatory genes and extrinsic mechanisms controlling arealization of the neocortex. *Curr Opin Neurobiol* **12**, 14-25.

O'Leary, D. D. and Sahara, S. (2008). Genetic regulation of arealization of the neocortex. *Curr Opin Neurobiol* **18**, 90-100.

O'Leary, D. D. and Terashima, T. (1988). Cortical axons branch to multiple subcortical targets by interstitial axon budding: implications for target recognition and "waiting periods". *Neuron* **1**, 901-910.

Peterburs, J. and Desmond, J. E. (2016). The role of the human cerebellum in performance monitoring. *Curr Opin Neurobiol* **40**, 38-44.

Petersen, S. C., Watson, J. D., Richmond, J. E., Sarov, M., Walthall, W. W. and Miller, D. M., 3rd (2011). A transcriptional program promotes remodeling of GABAergic synapses in Caenorhabditis elegans. *J Neurosci* **31**, 15362-15375.

Polleux, F., Dehay, C. and Kennedy, H. (1997). The timetable of laminar neurogenesis contributes to the specification of cortical areas in mouse isocortex. *J Comp Neurol* **385**, 95-116.

Porrero, C., Rubio-Garrido, P., Avendano, C. and Clasca, F. (2010). Mapping of fluorescent protein-expressing neurons and axon pathways in adult and developing Thy1-eYFP-H transgenic mice. *Brain Res* **1345**, 59-72.

Pourchet, O., Morel, M. P., Welniarz, Q., Sarrazin, N., Marti, F., Heck, N., Gallea, C., Doulazmi, M., Roig Puiggros, S., Moreno-Bravo, J. A., et al. (2021). Loss of floor plate Netrin-1 impairs midline crossing of corticospinal axons and leads to mirror movements. *Cell reports* **34**, 108654.

Proville, R. D., Spolidoro, M., Guyon, N., Dugue, G. P., Selimi, F., Isope, P., Popa, D. and Lena, C. (2014). Cerebellum involvement in cortical sensorimotor circuits for the control of voluntary movements. *Nat Neurosci* **17**, 1233-1239.

Puchades, M. A., Csucs, G., Ledergerber, D., Leergaard, T. B. and Bjaalie, J. G. (2019). Spatial registration of serial microscopic brain images to three-dimensional reference atlases with the QuickNII tool. *PLoS One* **14**, e0216796.

Schindelin, J., Rueden, C. T., Hiner, M. C. and Eliceiri, K. W. (2015). The ImageJ ecosystem: An open platform for biomedical image analysis. *Molecular reproduction and development* **82**, 518-529.

Schmahmann, J. D. and Pandya, D. N. (1997). Anatomic organization of the basilar pontine projections from prefrontal cortices in rhesus monkey. *J Neurosci* **17**, 438-458.

Shambes, G. M., Gibson, J. M. and Welker, W. (1978). Fractured somatotopy in granule cell tactile areas of rat cerebellar hemispheres revealed by micromapping. *Brain, behavior and evolution* **15**, 94-140.

Shepherd, G. M. (2009). Intracortical cartography in an agranular area. *Front Neurosci* **3**, 337-343.

Smart, I. H. (1984). Histogenesis of the mesocortical area of the mouse telencephalon. *J Anat* **138 (Pt 3)**, 537-552.

Stoodley, C. J. and Schmahmann, J. D. (2010). Evidence for topographic organization in the cerebellum of motor control versus cognitive and affective processing. *Cortex* **46**, 831-844.

Tomasch, J. (1968). The overall information carrying capacity of the major afferent and efferent cerebellar cell and fiber systems. *Confin Neurol* **30**, 359-367.

---- (1969). [The renal pelvis of the dromedary]. *Z Anat Entwicklungsgesch* **128**, 235-242.

Tomassy, G. S., De Leonibus, E., Jabaudon, D., Lodato, S., Alfano, C., Mele, A., Macklis, J. D. and Studer, M. (2010). Area-specific temporal control of corticospinal motor neuron differentiation by COUP-TFI. *Proc Natl Acad Sci U S A* **107**, 3576-3581.

Wang, Q., Ding, S. L., Li, Y., Royall, J., Feng, D., Lesnar, P., Graddis, N., Naeemi, M., Facer, B., Ho, A., et al. (2020). The Allen Mouse Brain Common Coordinate Framework: A 3D Reference Atlas. *Cell* **181**, 936-953 e920.

Welker, C. (1971). Microelectrode delineation of fine grain somatotopic organization of (SmI) cerebral neocortex in albino rat. *Brain Res* **26**, 259-275.

Woolsey, T. A. and Van der Loos, H. (1970). The structural organization of layer IV in the somatosensory region (SI) of mouse cerebral cortex. The description of a cortical field composed of discrete cytoarchitectonic units. *Brain Res* **17**, 205-242.

Zhou, C., Tsai, S. Y. and Tsai, M. J. (2001). COUP-TFI: an intrinsic factor for early regionalization of the neocortex. *Genes Dev* **15**, 2054-2059.

Zhou, H. M. and Walthall, W. W. (1998). UNC-55, an orphan nuclear hormone receptor, orchestrates synaptic specificity among two classes of motor neurons in Caenorhabditis elegans. *J Neurosci* **18**, 10438-10444.